Modulation of Stimuli-Responsiveness toward Acid Vapor between Real-Time and Write-Erase Responses Based on Conjugated Polymers Containing Azobenzene and Schiff Base Moieties

Taichi Kato, Masayuki Gon, Kazuo Tanaka* and Yoshiki Chujo

Department of Polymer Chemistry, Graduate School of Engineering, Kyoto University Katsura, Nishikyo-ku, Kyoto 615-8510, Japan

E-mail: tanaka@poly.synchem.kyoto-u.ac.jp

Key words: azobenzene; azomethine, acid sensor; chromism; π-conjugated polymer

Abstract

We developed three types of film-type stimuli-responsive polymers based on aza-substituted conjugated polymers involving azobenzene, **N_bith**, **N_fluo** and Schiff base moieties, **C_bith**. All polymer films showed bathochromic shifts in absorption spectra followed by chromic behaviors by fuming trifluoroacetic acid (TFA). In particular, we disclosed that there were three significant differences on acid detecting ability between azobenzene and Schiff base derivatives in terms of absorption wavelengths, stability, and proton holding time. The azobenzene polymers exhibited real-time responses toward vapor fuming, meanwhile write and erase chromic behaviors were reversibly accomplished with the Schiff base polymer by exposing to acid and amine vapor. Theoretical calculation revealed that red-shifted absorption bands should be induced by protonation on nitrogen atoms in the aza-substituted positions. Diverse responses through dynamic regulation of electronic properties of main-chain conjugation can be accomplished by introducing the aza-substituents in polymers.

Introduction

It has been recognized that conjugated polymers are a versatile platform for developing next generation of optoelectronic organic devices including wearable devices, huge flat display and so on because of designable optical and electronic properties, such as light absorption, emission and carrier-transport abilities as well as good material properties, such as film-formability, flexibility and lightness.[1–4] To receive further functions from polymers, the promising strategy is to introduce heteroatoms into polymer main-chains in π-conjugated polymers.[5–8] In particular, by utilizing electronic interaction between heteroatoms and main-chain conjugation as well as intrinsic environmental responsivity of heteroatoms, a wide variety of sensing materials having stimuli-responsive optical properties can be expected from heteroatom-containing conjugated systems.[9–11] For instance, we have proposed the idea on the material design based on an "element-block", which is the minimum functional units containing heteroatom, as a scaffold.[12–14] On the basis of this idea, various film-type sensors for detecting acid/base vapors,[15] reactive oxygen species[16] and mechanical stresses[17,18] were obtained with conjugated polymers involving boron "element-blocks" having environment-responsive luminochromic characters. Except for our examples, although many researchers have realized unique sensing materials with heteroatom-containing conjugated polymers, in order to obtain advanced sensing materials, establishment of precise controls of stimuli-responsivity toward environmental changes and external stimuli is still one of relevant topics in this research field.[19–24]

We have recently shown the protocol for selectively lowering energy levels of each

frontier molecular orbital (FMO) by replacing the skeletal carbon to nitrogen where one of FMOs is distributed.[25] By applying this aza-substitution protocol for lowering lowest unoccupied molecular orbitals (LUMOs) of conventional chromophores, light-absorbing materials in the longer wavelength region can be obtained.[26–30] The strategy for selective control of FMO was also suggested by Bunz *et al.* by cross-conjugated cruciform fluorophores.[31] In general, extension and restriction of π-conjugation and electron-donating and withdrawing interaction are the conventional manners for modulating electronic properties of polymers, meanwhile significant changes are accomplished only by replacing carbon to heteroatom in our design scheme. Moreover, by boron complexation, further red-shifts in optical spectra are enhanced.[32] Consequently, near-infrared absorption and emission were observed from the aza-substituted polymers.[33] These results mean that the nitrogen atom replaced from the skeletal carbon can play a critical role in perturbation of electronic structures of conjugated polymers. From this fact, we presumed that the further regulation of electronic properties of main-chain conjugation might be feasible by using the nitrogen atom as a key point. On the basis of this speculation, we designed the aza-substituted polymers from poly(*p*-phenylenevinylene),[34] which is one of commodity conjugated polymers for organic optoelectronic devices, for demonstrating dynamic regulation of optical properties by environmental changes.

We herein report the design and syntheses for aza-substituted conjugated polymers possessing environment responsiveness. Based on the azobenzene[32,33,35–40] and Schiff base[41–46] structures, we prepared copolymers with fluorene and bithiophene units. We successfully obtained three types of polymer films and evaluated stimuli responsivity. It

was demonstrated that the synthesized polymer films can exhibit drastic color changes by acid-vapor fuming. In particular, depending on the number of aza-substitution at the main chain, absorption wavelengths, stability, and proton holding time can be tuned. Moreover, we obtained the film-type sensor which can discriminate the type of strong acids. From the mechanistic studies in experimental as well as theoretical, it was shown that protonation at the nitrogen atom should be responsible for color changes. We demonstrate in this research that the aza-substitution at the polymer chains should be the effective design strategy for introducing environmental sensitivity into conjugated polymers.

Scheme 1 shows the synthesis of copolymers consisting of azobenzene and *N*-benzylideneaniline units. Initially, we synthesized azobenzene and *N*-benzylideneaniline monomers using an oxidation coupling reaction[47] and a classical imine formation reaction,[48] respectively. Polymerizations were carried out with 5,5′-bis(trimethylstannyl)-3,3′-didodecyl-2,2′-bithiophene (**6**) or 2,7-bis(trimethylstannyl)-9,9-didodecylfluorene (**7**) in the catalytic system of $Pd_2(dba)_3$ (dba = dibenzylideneacetone) using 2-dicyclohexylphosphino-2′,4′,6′-triisopropylbiphenyl (XPhos) as a phosphine ligand to obtain the polymers. Due to extremely-low solubility, we were not able to obtain the azomethine-fluorene copolymer (**C_fluo**). The number-average molecular weight (M_n) and weight-average molecular weight (M_w) were determined by a gel permeation chromatography (GPC) with $CHCl_3$ as an eluent with polystyrene standards (**C_bith** (isolated yield: 70%, M_n = 13,000, M_w/M_n = 2.2), **N_bith** (isolated yield: 96%, M_n =

23,000, M_w/M_n = 2.6), and **N_fluo** (isolated yield: 91%, M_n = 7,000, M_w/M_n = 3.4). The structures of all new compounds were confirmed by ^{1}H and ^{13}C NMR spectroscopy and matrix assisted laser desorption ionization-time of flight mass spectrometry (MALDI-TOFMS) (the detailed synthetic procedures and NMR data are shown in the Supporting Information, Charts S1–S8). Redox activity was confirmed by cyclic voltammetry (Chart S9). The synthesized polymers showed good thermal stability (T_d > 400 ℃) according to the data from thermogravimetric analyses (Figures S3 and S4 and Table S4) and resistance toward air and moisture similarly to conventional conjugated polymers. Additionally, the polymers have solubility toward conventional organic solvents, such as chloroform, dichloromethane and tetrahydrofuran. Thus, film samples can be obtained via a spin-coating method and used in further experiments. Also, the polymers were fractionated on a recycling preparative high performance liquid chromatography (HPLC) to investigate molecular weight dependency of optical properties. The molecular weights of the fractionated polymers were also determined by GPC (Figure S1 and Tables S1–S3).

To examine electronic structures of the synthesized polymers in the ground state, UV–vis absorption properties were evaluated in various dilute solutions (1.0×10^{-5} M) with mixed solvents of $CHCl_3$/each solvent (1/99, v/v). It was revealed that there was almost no solvent dependency in these polymers (Figure S2). We next surveyed responses to acid with trifluoroacetic acid (TFA) in solution. The absorption spectra of **N_bith** and **N_fluo** including the azobenzene moieties did not change even though the concentration of TFA reached 50 mM (5000 equivalents per unit of azo moieties) (Figures S5a and S5b). These results indicate that azobenzene moiety is not protonated

and hardly decomposed even in the presence of strong acid. In contrast, the absorption bands from **C_bith** including the Schiff base moiety were blue-shifted as the concentration of TFA increasing (Figure S5c). It is implied that **C_bith** might be gradually degraded until the spectrum variation has finished. Finally, the polymer was completely hydrolyzed at the concentration of TFA reached 10 mM (1000 equivalents to the samples). This hydrolysis is likely because it is well known that an imine linkage is easily hydrolyzed to amine and carbonyl compounds in the presence of acid.[49,50]

Next, to examine the optical properties in the film state, we prepared spin-coated thin films on the quartz substrate (0.9 cm×5 cm) with the $CHCl_3$ solutions (0.15 mL, concentration: 1 mg/300 μL, 1000 rpm, 30 sec) and measured UV–vis absorption spectra of the three polymers in film state in the case of either exposing (**N_bith** and **N_fluo**) and after exposed TFA (**C_bith**) (Figure 1). Unlike optical properties in dilute solutions, these polymers showed red-shifted absorption bands and subsequently color change by fuming TFA vapor. In the comparison of the degree of peak shifts with **N_bith** and **N_fluo**, **N_bith** exhibited a larger change (from 460 nm to 890 nm) than that of **N_fluo** (from 430 nm to 730 nm). These red-shifts were observed identically irrespective of molecular weight (Figure S6). It is proposed that the nitrogen atoms in the azobenzene and the Schiff base moieties should be protonated with TFA vapor in film state, resulting in bathochromic shifts in absorption spectra. This speculation is supported by DFT calculation in the following section.

There are several differences between the *N*-benzylideneaniline and azobenzene derivatives. First, the absorption of **C_bith** had a shorter wavelength than **N_bith**. This

tendency was consistent with previous reports.[51,52] Similarly, the protonated state of **C_bith** showed a shorter absorption wavelength than that of **N_bith** (Figure S7). Second, the degree of stability of chemical bonds constructed by azobenzene (**N_bith** and **N_fluo**) and Schiff base moieties (**C_bith**) to TFA vapor was different. We prepared drop-casted films on slide glasses (2.5 cm×7.5 cm, 1.5 mg/glass). After exposure to TFA vapor for 3 s, they were redissolved in $CHCl_3$, and the solvent was removed by evaporation and dried under vacuum. Then NMR and GPC measurements were performed with these samples. Accordingly, in their NMR spectra (Figures S8a and S8b) and GPC chromatograms (Figures S9a and S9b, Tables S5 and S6), we hardly detected significant changes before and after exposing TFA, indicating that **N_bith** and **N_fluo** were hardly degraded with exposing TFA vapor, similarly to the solution samples. It should be emphasized that **C_bith** was slightly degraded to aldehyde and amine according to its NMR spectra and GPC chromatograms, clearly indicating that stability of the imine unit toward acid vapor can be enhanced in the film state (Figures S8c and S9c, Tables S7 and S8). It is likely that acid-catalyzed hydrolysis at the imine unit should be suppressed in film because the hydrolysis proceeds in multi-steps and reaches equilibrium. Then, obtained entropy should be smaller in film than in solution. Therefore, it should take longer time to finish the hydrolysis than the single-step protonation by TFA.

It is worth noting that how long they retain protons in film state is extremely different (Figure 2). **N_bith** and **N_fluo** including azobenzene moieties were able to retain protons only under TFA vapor. As shown in Figure 2a and movie 1, the films returned to their original color as soon as they were liberated to the atmosphere. Therefore, the

measurements of protonated **N_bith** and **N_fluo** were performed by placing the film on cotton impregnated with 150 μL of TFA in a closed cell as shown in Figure S10. On the other hand, once **C_bith** was exposed to TFA vapor and subsequently left in the atmosphere, the film sample surprisingly maintained the color for about 1 h in the absence of TFA (Figure 2b and movie 2). Then, **C_bith** film was returned to its original color at last (Figure 2c). In particular, **C_bith** also was able to be restored immediately to its original color by exposure to triethyl amine (NEt_3) vapor (movie 3). We performed UV–vis measurements by repeating cycles of exposure to TFA vapor and to NEt_3 vapor. As a result, it was confirmed that the blue-shift caused by the decomposition was scarcely observed and the spectral shape was nearly the same as that of the initial pristine film, and the film was reusable at least three times (Figure 3). These results mean that the film-type sensors which express not only real-time changes but also write-erase responses can be obtained by modulating the number of aza-substitution.

Finally, we examined influence of other acid species on absorption properties of films. We used **N_fluo** (without sulfur atom) that is exactly identified that protonation on the nitrogen atom in azobenzene moiety induced absorption red-shift (Table 1 and Figures S29 and S30). Different responsiveness was observed depending on the acid types. In the case of nitric acid (HNO_3), the film showed the same spectral change as that with TFA (Figure S30). In addition, when the film was dipped into the acid, the same responsiveness was detected (Figure S29c). By using sulfuric acid (H_2SO_4), the film showed red-shift only when it was dipped into the acid (Figure S29b). When acetic acid (CH_3COOH), which doesn't have enough small pK_a value to induce protonation at the nitrogen atom in azobenzene moiety, is used, significant changes were hardly obtained

(Figure S29d). It is noteworthy that in the cases of hydrochloric acid (HCl) and hydrobromic acid (HBr), although their pK_a values are much lower than TFA, **N_fluo** did not show red-shift either on vapor or dipped into the acids (Figure S29a). It was speculated that this result was due to the high water content. Nakano *et al.* reported that H_2O in breath caused deprotonation, and the blue-shift (from the protonated state to the deprotonated state) was observed.[53] Therefore, we supposed that protonated state could be highly sensitive to H_2O, and **N_fluo** did not show red-shift in the case of HCl and HBr. These data represent that the type of acids can discriminate by selecting the aza-substitution manner at the main-chain conjugation.

To elucidate the effect of the protonation on optical properties, we performed theoretical calculations to estimate the electronic structures and characters of the three polymers. Density functional theory (DFT) and time-dependent DFT (TD-DFT) calculations were performed at (TD-)B3LYP/6-31+G(d,p) and (TD-)CAM-B3LYP/6-31+G(d,p) level of theory. Initially, we optimized the structures of neutral state (**N_bith'**, **N_fluo'** and **C_bith'**) and protonated state (**N_bith+'**, **N_fluo+'** and **C_bith+'**) which are model compounds of three polymers in the ground S_0 states at B3LYP/6-31+G(d,p) and CAM-B3LYP/6-31+G(d,p) levels (Figures S11–S14). In these calculations, dodecyl groups were changed to methyl groups for simplification in the calculation. In comparison between Figures S11 and S12 and between Figures S13 and S14, it is suggested that, in both functions, protonation on nitrogen atom potentially increases the planarity of the entire molecules probably because of contribution of quinoid-type structures observed in HOMO−1 (Figures S17–S28) (HOMO: highest occupied molecular orbital). Next, we calculated the energy of

the S_0–S_1 and S_0–S_2 transitions with optimized geometries in the S_0 states by TD-DFT at B3LYP/6-31+G(d,p) and CAM-B3LYP/6-31+G(d,p) levels (Tables S9–S14). Accordingly, rationality of these functions was mutually proved and the optical properties of the polymers were qualitatively reproduced. That is, the trends in optical properties were well reproduced in both functions. In particular, comparing the experimental data and the calculated values (Figures S15 and S16), it is clearly revealed that protonation on nitrogen atom in azobenzene and Schiff base moieties induced absorption red-shift.

Furthermore, we analyzed frontier molecular orbitals (FMOs) to discuss the electronic states of the polymers. In Figures S17–S28, we summarize the FMOs that have the main contributions in the S_0–S_1 and S_0–S_2 transitions. In **N_bith'** and **N_fluo'**, the S_0–S_1 transitions were assigned to the forbidden n–π* transitions and the S_0–S_2 transitions were assigned to the permitted π–π* transitions like common azobenzene derivatives.[54] Meanwhile, both of the S_0–S_1 and the S_0–S_2 transitions in **N_bith+'** and **N_fluo+'** were assigned to π–π* transitions. In the case of **C_bith'** and **C_bith+'**, both of the S_0–S_1 and the S_0–S_2 transitions are assigned to the permitted π–π* transitions. Focusing on the energies of HOMOs and LUMOs, both are lowered by protonation, while the energies of LUMOs are significantly reduced than HOMOs, leading to narrow energy gaps. Therefore, their absorptions were red-shifted on protonation.

Conclusion

We synthesized three copolymers containing azobenzene and Schiff base moieties with bithiophene and fluorene. These polymers showed red-shift in absorption spectra by exposing acid vapors in film. There are three significant differences between azobenzene and Schiff base derivatives in terms of absorption wavelengths, stability, and proton holding time. In particular, **C_bith** including Schiff base moieties was able to hold and release proton reversibly by fuming acid and amine vapor. In addition, it was found that **N_fluo** film was sensitive to acid types in terms of boiling point, water content, and pK_a value. From theoretical calculation, it was supported that protonation on the nitrogen atom in azobenzene and Schiff base moieties induced absorption red-shift. This study demonstrate not only feasibility of azobenzene and Schiff base as a platform for constructing an acid responsive film but also applicability of aza-substituted conjugated polymers as a film-type sensing material.

Acknowledgements

This work was partially supported by a Grant-in-Aid for Early-Career Scientists (for M.G.) (JSPS KAKENHI Grant numbers 20K15334), for Scientific Research (B) (for K.T), (JP17H03067), for Scientific Research on Innovative Areas “New Polymeric Materials Based on Element-Blocks (No.2401)” (JP24102013) and for Challenging Research (Pioneering) (JP18H05356).

Scheme 1. Syntheses of **N_bith**, **N_fluo**, and **C_bith**

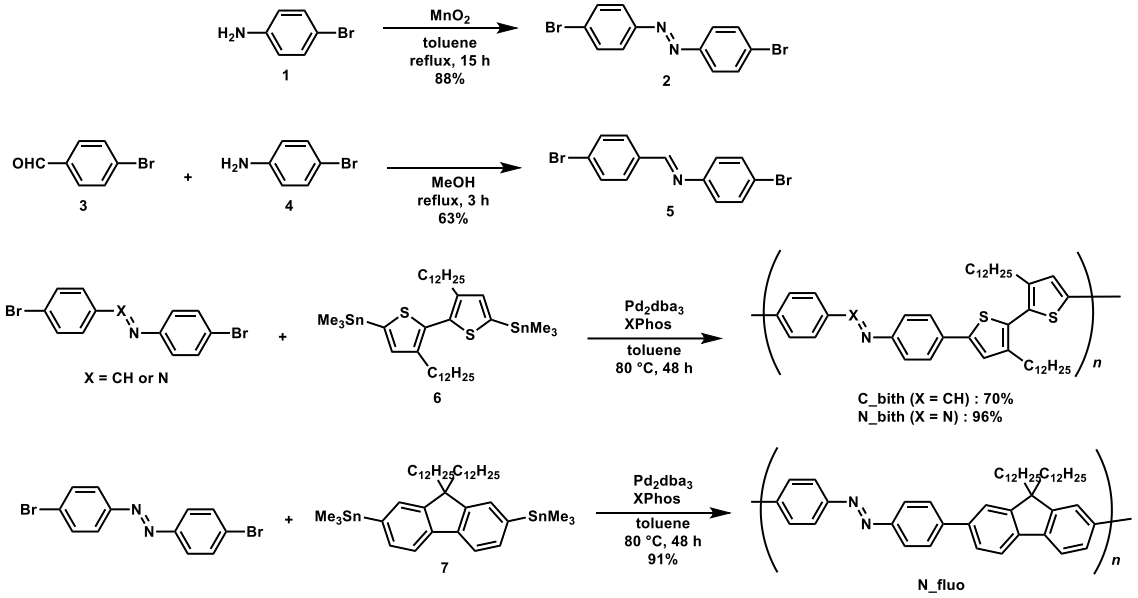

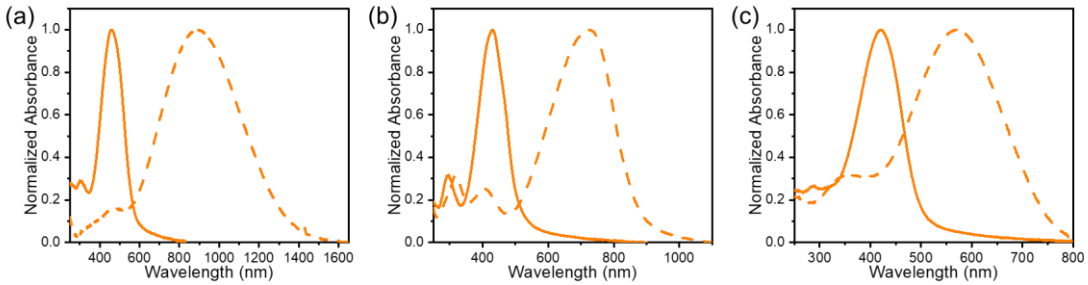

Figure 1. UV–vis absorption spectra in films of (a) **N_bith** (solid line: pristine film, dashed line: exposed with TFA vapor for 3 s), (b) **N_fluo** (solid line: pristine film, dashed line: under TFA vapor), and (c) **C_bith** (solid line: pristine film, dashed line: after exposed TFA vapor). These film samples were prepared via the spin-coating (1000 rpm, 30 sec) on the quartz substrate with $CHCl_3$ (1 mg/300 μL).

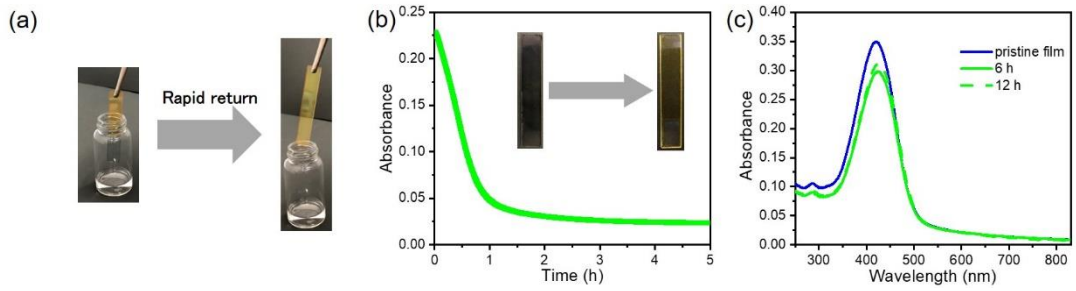

Figure 2. (a) Photographic images of rapid response (<<1 sec) against TFA vapor in a sample bottle (**N_bith** (this photograph) and **N_fluo** showed same responses). (b) Time tracking absorbance spectrum of **C_bith** measured at 598 nm per 10 s after exposure to TFA vapor. (c) UV–vis absorption spectra in the film state of **C_bith** (blue solid line: pristine film, green solid line: 6 h after exposure to TFA vapor and left in the atmosphere, and green dashed line: 12 h after exposure to TFA vapor and left in the atmosphere).

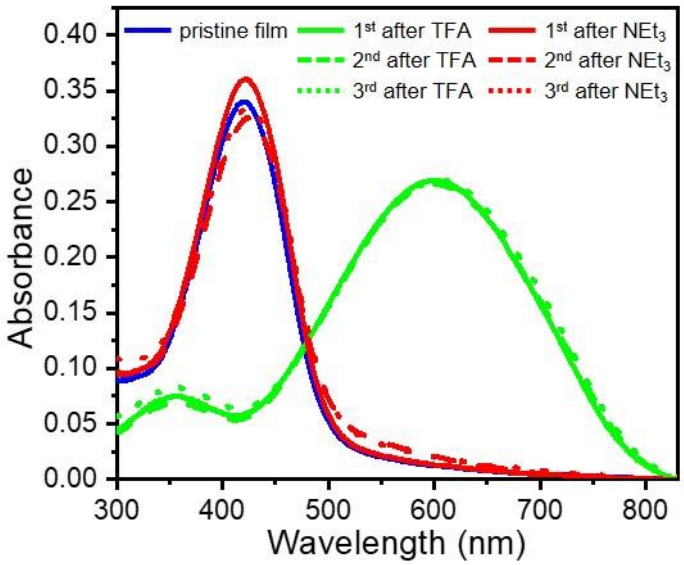

Figure 3. UV–vis absorption spectra of three cycles of repeated TFA and NEt_3 vapor exposure to the **C_bith** film. Blue solid line: pristine film, green solid line: first cycle after TFA vapor exposure, green dashed line: second cycle after TFA vapor exposure, green dotted line: third cycle after TFA vapor exposure, red solid line: first cycle after NEt_3 vapor exposure, red dashed line: second cycle after NEt_3 vapor exposure, and red dotted line: third cycle after NEt_3 vapor exposure.

Table 1. The result of **N_fluo**'s response to various acids (×: not response, ○: response)

	pK_a	Concentration /wt%	b.p. /°C	Dip	Vapor
HBr	−9.0	47~49	−66	×	×
HCl	−8.0	35~37	−85	×	×
H_2SO_4	−3.0	95	337	○	×
HNO_3	−1.3	69~70	83	○	○
CF_3COOH	−0.25	98	72	○	○
CH_3COOH	4.76	99.0+	118	×	×

4. Reference

[1] A. X. Chen, A. T. Kleinschmidt, K. Choudhary, D. J. Lipomi, *Chem. Mater.* **2020**, *32*, 7582.

[2] A. Facchetti, *Chem. Mater.* **2011**, *23*, 733.

[3] J.-L. Brédas, D. Beljonne, V. Coropceanu, J. Cornil, *Chem. Rev.* **2004**, *104*, 4971.

[4] T. Chiba, Y.-J. Pu, J. Kido, *J. Mater. Chem. C* **2015**, *3*, 11567.

[5] K. Tanaka, Y. Chujo, *Macromol. Rapid Commun.* **2012**, **33**, 1235.

[6] M. Hissler, P. Dyer, R. Réau, *Coord. Chem. Rev.* **2003**, *244*, 1.

[7] X. Yin, J. Liu, F. Jäkle, *Chem. Eur. J.* **2021**, *27*, 2973.

[8] J. Crassous, R. Réau, *Dalton Trans.* **2008**, 6865.

[9] K. Tanaka, Y. Chujo, *NPG Asia Mater.* **2015**, *7*, e223.

[10] N. Matsumi, Y. Chujo, *Polym. J.* **2008**, *40*, 77.

[11] M. Miyata, Y. Chujo, *Polym. J.* **2002**, *34*, 967.

[12] Y. Chujo, K. Tanaka, *Bull. Chem. Soc. Jpn.* **2015**, *88*, 633.

[13] M. Gon, K. Tanaka, Y. Chujo, *Polym. J.* **2018**, *50*, 109.

[14] K. Tanaka, Y. Chujo, *Polym. J.* **2020**, *52*, 555.

[15] R. Yoshii, A. Hirose, K. Tanaka, Y. Chujo, *J. Am. Chem. Soc.* **2014**, *136*, 18131.

[16] A. Hirose, K. Tanaka, R. Yoshii, Y. Chujo, *Polym. Chem.* **2015**, *6*, 5590.

[17] R. Yoshii, K. Suenaga, K. Tanaka, Y. Chujo, *Chem. Eur. J.* **2015**, 21, 7231.

[18] K. Suenaga, K. Uemura, K. Tanaka, Y. Chujo, *Polym. Chem.* **2020**, *11*, 1127.

[19] S. W. Thomas, G. D. Joly, T. M. Swager, *Chem. Rev.* **2007**, *107*, 1339.

[20] Y. L. Pak, Y. Wang, Q. Xu, *Coord. Chem. Rev.* **2021**, *433*, 213745.

[21] A. Sundararaman, M. Victor, R. Varughese, F. Jäkle, *J. Am. Chem. Soc.* **2005**, *127*, 13748.

[22] L.-J. Fan, W. E. Jones, *J. Am. Chem. Soc.* **2006**, *128*, 6784.

[23] C. Bathula, O. Henry, A. Kumar K, S. K, A. Jana, I. Rabani, J.-H. Choi, J.-H. Jeon, H.-S. Kim, *Dyes Pigm.* **2021**, *184*, 108847.

[24] N. Zehra, A. Kalita, A. H. Malik, U. Barman, M. Adil Afroz, P. K. Iyer, *ACS Sens.* **2020**, *5*, 191.

[25] K. Tanaka, Y. Chujo, *Chem. Lett.* **2021**, *50*, 269.

[26] H. Watanabe, M. Hirose, K. Tanaka, K. Tanaka, Y. Chujo, *Polym. Chem.* **2016**, *7*, 3674.

[27] H. Watanabe, M. Hirose, K. Tanaka, Y. Chujo, *Chem. Commun.* **2017**, *53*, 5036.

[28] H. Watanabe, K. Tanaka, Y. Chujo, *J. Org. Chem.* **2019**, *84*, 2768.

[29] H. Watanabe, J. Ochi, K. Tanaka, Y. Chujo, *Eur. J. Org. Chem.* **2020**, 777.

[30] H. Watanabe, Y. Kawano, K. Tanaka, Y. Chujo, *Asian J. Org. Chem.* **2020**, *9*, 259.

[31] A. J. Zucchero, P. L. McGrier, U. H. F. Bunz, *Acc. Chem. Res.* **2010**, 43, 397.

[32] M. Gon, K. Tanaka, Y. Chujo, *Angew. Chem. Int. Ed.* **2018**, *57*, 6546.

[33] J. Wakabayashi, M. Gon, K. Tanaka, Y. Chujo, *Macromolecules* **2020**, *53*, 4524.

[34] A. J. Blayney, I. F. Perepichka, F. Wudl, D. F. Perepichka, *Isr. J. Chem.* **2014**, *54*, 674.

[35] H. M. D. Bandara, S. C. Burdette, *Chem. Soc. Rev.* **2012**, *41*, 1809.

[36] E. Merino, *Chem. Soc. Rev.* **2011**, *40*, 3835.

[37] A. Izumi, R. Nomura, T. Masuda, *Macromolecules* **2001**, *34*, 4342.

[38] A. Dirksen, E. Zuidema, R. M. Williams, L. De Cola, C. Kauffmann, F. Vögtle, A. Roque, F. Pina, *Macromolecules* **2002**, *35*, 2743.

[39] Y. A. Mikheev, L. N. Guseva, Y. A. Ershov, *Russ. J. Phys. Chem. A* **2015**, *89*,

224.

[40] S. Guo, K. Matsukawa, T. Miyata, T. Okubo, K. Kuroda, A. Shimojima, *J. Am. Chem. Soc.* **2015**, *137*, 15434.

[41] Y. Jia, J. Li, *Chem. Rev.* **2015**, *115*, 1597.

[42] P. G. Cozzi, *Chem. Soc. Rev.* **2004**, *33*, 410.

[43] J. L. Segura, M. J. Mancheño, F. Zamora, *Chem. Soc. Rev.* **2016**, 45, 5635.

[44] Z. Chen, K. Wang, X. Hu, P. Shi, Z. Guo, H. Zhan, *ACS Appl. Mater. Interfaces* **2021**, *13*, 1145.

[45] S. Ohtani, M. Gon, K. Tanaka, Y. Chujo, *Chem. Eur. J.* **2017**, *23*, 11827.

[46] S. Ohtani, M. Gon, K. Tanaka, Y. Chujo, *Macromolecules* **2019**, *52*, 3387.

[47] W. Zhang, K. Yoshida, M. Fujiki, X. Zhu, *Macromolecules* **2011**, *44*, 5105.

[48] Q. Liu, G. Li, Z. Tang, L. Chen, B. Liao, B. Ou, Z. Zhou, H. Zhou, *Mater. Chem. Phys.* **2017**, *186*, 11.

[49] M. E. Belowich, J. F. Stoddart, *Chem. Soc. Rev.* **2012**, *41*, 2003.

[50] A. C. Dash, B. Dash, S. Praharaj, *J. Chem. Soc., Dalton Trans.* **1981**, 2063.

[51] Y. Wang, J. Ma, Y. Jiang, *J. Phys. Chem. A* **2005**, *109*, 7197.

[52] C.-L. Liu, F.-C. Tsai, C.-C. Chang, K.-H. Hsieh, J.-L. Lin, W.-C. Chen, *Polymer* **2005**, *46*, 4950.

[53] Y. Kitamura, R. Ichikawa, H. Nakano, *Mater. Chem. Front.* **2018**, *2*, 90.

[54] D. B. Konrad, G. Savasci, L. Allmendinger, D. Trauner, C. Ochsenfeld, A. M. Ali, *J. Am. Chem. Soc.* **2020**, *142*, 6538.

TOC

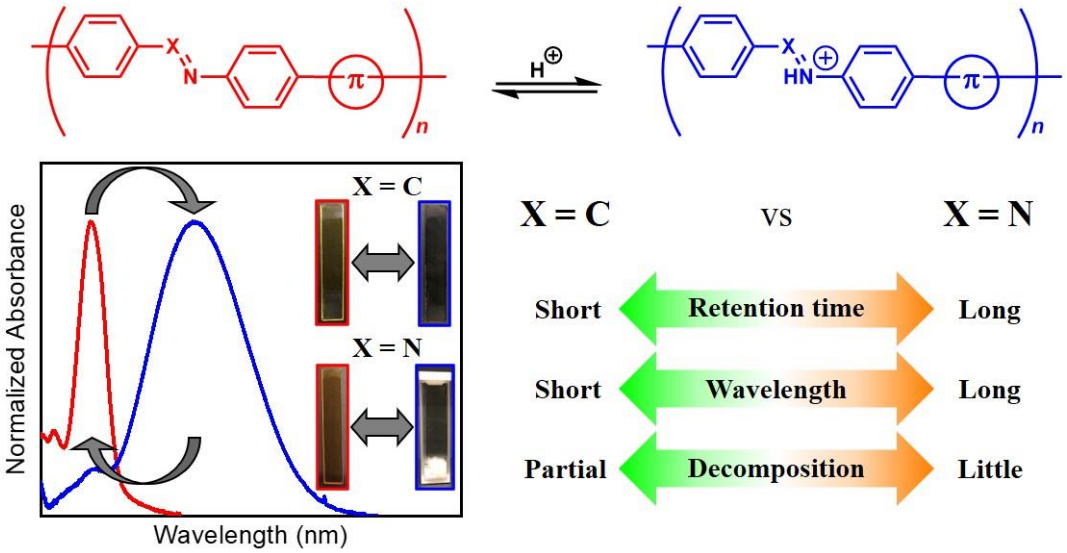
X
N
π
n
H
X
HN
π
n
X = C
X = N
Normalized Absorbance
Wavelength (nm)
X = C
vs
X = N
Short
Retention time
Long
Short
Wavelength
Long
Partial
Decomposition
Little

Supporting Information

Modulation of Stimuli-Responsiveness toward Acid Vapor between Real-Time and Write-Erase Responses Based on Conjugated Polymers Containing Azobenzene and Schiff Base Moieties

Taichi Kato, Masayuki Gon, Kazuo Tanaka* and Yoshiki Chujo

Department of Polymer Chemistry, Graduate School of Engineering, Kyoto University

Katsura, Nishikyo-ku, Kyoto 615-8510, Japan

E-mail: tanaka@poly.synchem.kyoto-u.ac.jp

Contents page

General

^{1}H and ^{13}C NMR spectra were recorded on JEOL AL400 instruments at 400 and 100 MHz, respectively. Samples were analyzed in $CDCl_3$, CD_2Cl_2. The chemical shift values were expressed relative to Me_4Si for ^{1}H and ^{13}C NMR as an internal standard in $CDCl_3$. Matrix Assisted Laser Desorption ionization-Time of Flight Mass Spectrometry (MALDI-TOFMS) was performed at the Technical Support Office (Department of Synthetic Chemistry and Biological Chemistry, Graduate School of Engineering, Kyoto University), and the MALDI-TOFMS spectrum were obtained on a Bruker Daltonics ultrafleXtreme. UV–vis spectra were recorded on a SHIMADZU UV-3600 spectrophotometer, and samples were analyzed at room temperature. Gel permeation chromatography (GPC) was carried out on a TOSOH G3000HXI system equipped with three consecutive polystyrene gel columns (TOSOH gels: α-4000, α-3000, α-2500) using chloroform as an eluent after calibration with standard polystyrene samples. Polymer fractionation was carried out on a Recycling Preparative HPLC (LC-9204, Japan Analytical Industry Co., Ltd.). Thermogravimetric analyses (TGA) were recorded on a Hitachi High-Tech Science Corp. STA7200RV. The measurements were performed under the following condition. First, the temperature was raised to 100 °C at a rate of 10 °C/min and maintained at the temperature for 10 minutes. Next, the temperature was lowered to 30 °C at a rate of 10 °C/min and maintained at the temperature for 10 minutes. Finally, the measurements were carried out and recorded at a heating rate of 10 °C/min. Cyclic voltammetry (CV) was carried out on a BASALS-Electrochemical-Analyzer Model 600D with a grassy carbon working electrode, a Pt counter electrode, an Ag/AgCl reference electrode, and the ferrocene/ferrocenium (Fc/Fc+) external reference at a scan rate of 0.1 V s^{-1}.

Materials

Commercially available compounds used without purification:

4-Bromoaniline (Tokyo Chemical Industry Co, Ltd.)

4-Bromobenzaldehyde (Tokyo Chemical Industry Co, Ltd.)

$Pd_2(dba)_3$ (dba = dibenzylideneacetone) (Tokyo Chemical Industry Co, Ltd.)

2-Dicyclohexylphosphino-2′,4′,6′-triisopropylbiphenyl (XPhos) (Strem Chemicals, Inc.)

Commercially available solvents:

Toluene (deoxidized grade, FUJIFILM Wako Pure Chemical Industries, Ltd.)

MeOH (Wako Pure Chemical Industries, Ltd.)

Compounds prepared as described in the literatures:

1,2-Bis(4-bromophenyl)diazene (**2**)[1]

4-Bromo-*N*-[(4-bromophenyl)methylene]-benzenamine (**5**)[2]

5,5′-Bis(trimethylstannyl)-3,3′-didodecyl-2,2′-bithiophene (**6**)[3][4]

2,7-Bis(trimethylstannyl)-9,9-didodecylfluorene (**7**)[5]

Synthetic procedures and characterization

Synthesis of **N_bith**

A mixture of 1,2-bis(4-bromophenyl)diazene (**2**) (106 mg, 0.312 mmol), 5,5′-bis(trimethylstannyl)-3,3′-didodecyl-2,2′-bithiophene (**6**) (259 mg, 0.312 mmol), XPhos (8.9 mg, 0.018 mmol), $Pd_2(dba)_3$ (8.6 mg, 0.0094 mmol) was placed in a round-bottom flask equipped with a magnetic stirring bar. After degassing and filling N_2 three times, toluene (8.0 mL) was added to the mixture. The reaction was carried out at 80 °C for 48 h. atmosphere. After cooling to room temperature, the solution was purified by short column chromatography on SiO_2 and poured into a large amount of $CHCl_3$ to collect the polymer by filtration. The obtained polymer was redissolved in a small amount of $CHCl_3$, and then the product was reprecipitated from MeCN. The precipitation was collected with filtration and washed with MeCN repeatedly. The polymer was dried under vacuum to afford **N_bith** (204 mg, 96%) as a red solid.

M_n = 23,000, M_w = 59,000, M_w/M_n = 2.6. ^{1}H NMR ($CDCl_3$, 400 MHz) δ 7.97 (d, J = 8.0 Hz, 4H), 7.77 (d, J = 8.0 Hz, 4H), 7.35 (s, 2H), 2.62 (m, 4H), 1.65 (m, 4H), 1.24 (m, 36H), 0.87 (t, J = 6.4 Hz, 6H) ppm; ^{13}C NMR ($CDCl_3$, 100 MHz) δ 151.9, 144.0, 142.9, 136.7, 129.4, 126.0, 125.9, 123.7, 32.0, 30.7, 29.7, 29.7, 29.6, 29.5, 29.4, 29.2, 22.7, 14.1 ppm.

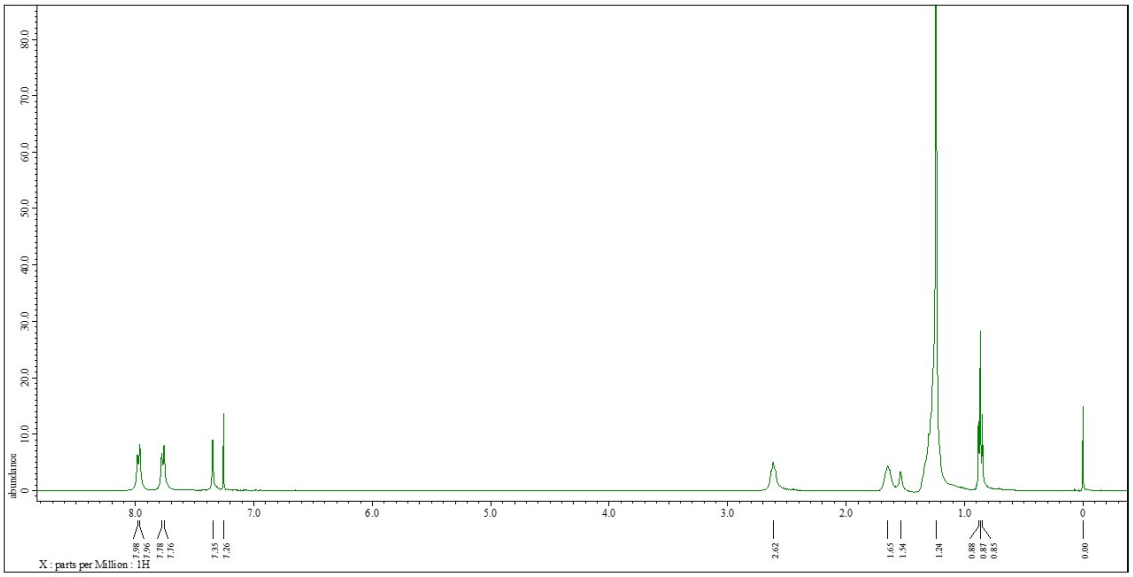

Chart S1. ^{1}H NMR spectrum of **N_bith** in $CDCl_3$.

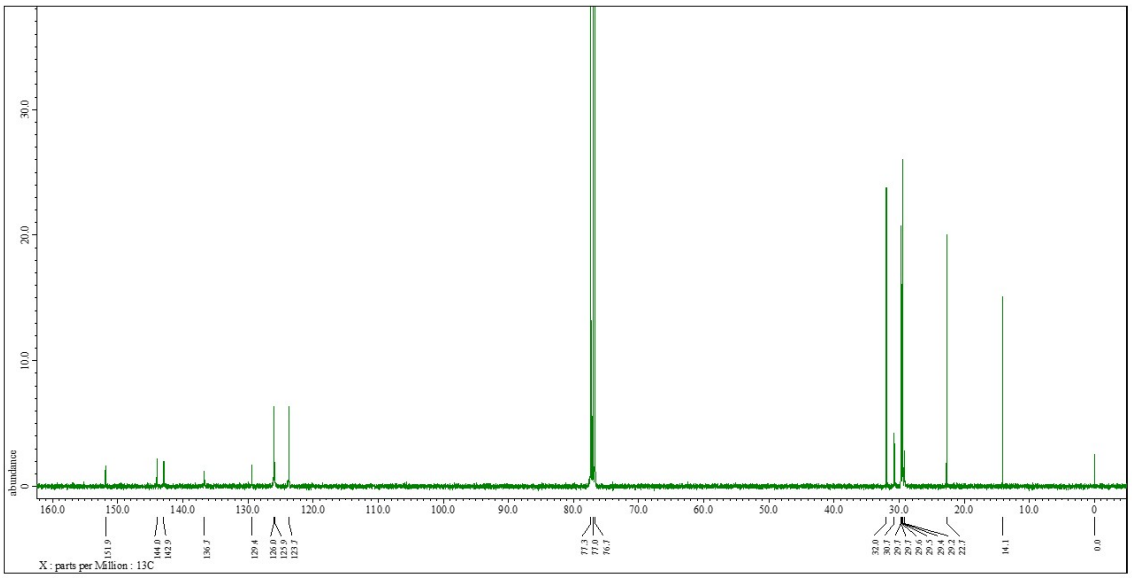

Chart S2. ^{13}C NMR spectrum of **N_bith** in $CDCl_3$.

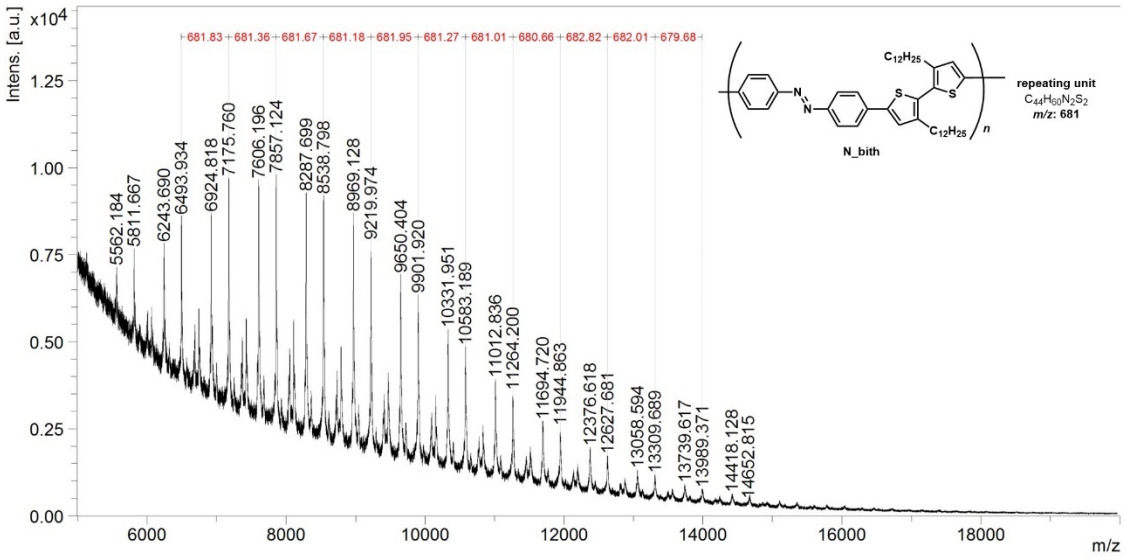

Chart S3. MALDI-TOFMS spectrum of **N_bith** (matrix: DCTB+Ag).

Synthesis of **N_fluo**

A mixture of 1,2-bis(4-bromophenyl)diazene (**2**) (84.1 mg, 0.248 mmol), 2,7-bis(trimethylstannyl)-9,9-didodecylfluorene (**7**) (205 mg, 0.248 mmol), XPhos (7.1 mg, 0.015 mmol), $Pd_2(dba)_3$ (6.8 mg, 0.0074 mmol) was placed in a round-bottom flask equipped with a magnetic stirring bar. After degassing and filling N_2 three times, toluene (10.0 mL) was added to the mixture. The reaction was carried out at 80 °C for 48 h. atmosphere. After cooling to room temperature, the solution was purified by short column chromatography on SiO_2 and poured into a large amount of $CHCl_3$ to collect the polymer by filtration. The obtained polymer was redissolved in a small amount of $CHCl_3$, and then the product was reprecipitated from MeCN. The precipitation was collected with filtration and washed with MeCN repeatedly. The polymer was dried under vacuum to afford **N_fluo** (154 mg, 91%) as a red solid.

M_n = 7,000, M_w = 23,000, M_w/M_n = 3.4. ^{1}H NMR ($CDCl_3$, 400 MHz) δ 8.08 (m, 4H), 7.86 (m, 6H), 7.70 (m, 4H), 2.12 (br, 2H), 1.56 (br, 3H), 1.25−1.10 (m, 36H), 0.85 (br, 9H) ppm; ppm; ^{13}C NMR ($CDCl_3$, 100 MHz) δ 152.0, 151.9, 144.1, 140.6, 127.8, 126.3, 123.5, 121.5, 120.3, 55.5, 40.4, 31.9, 29.6, 29.6, 29.6, 29.6, 29.3, 29.2, 23.8, 22.9, 22.7, 14.1 ppm.

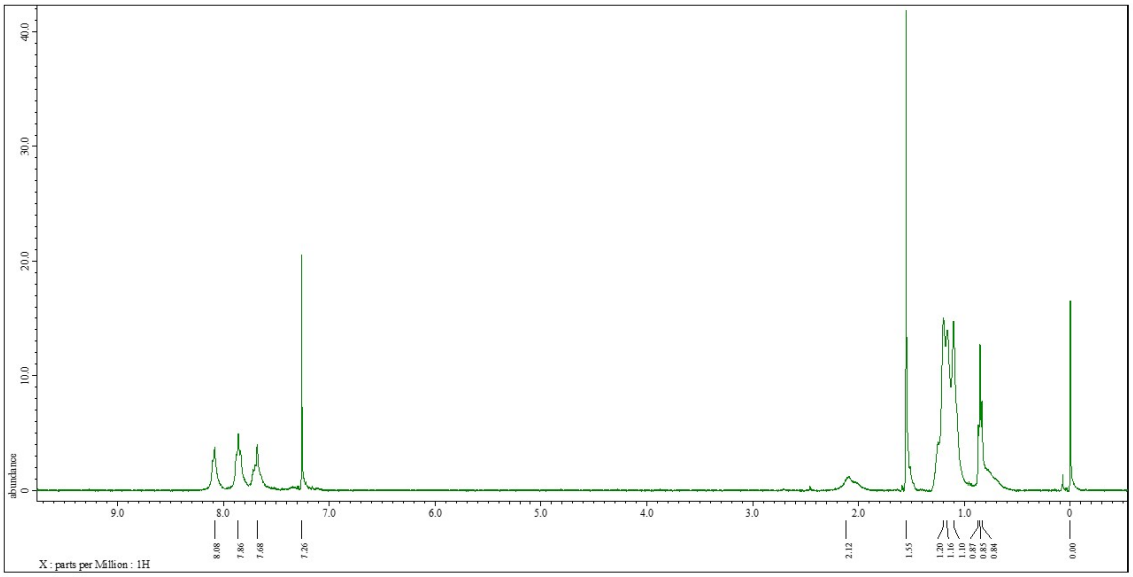

Chart S4. ^{1}H NMR spectrum of **N_fluo** in $CDCl_3$.

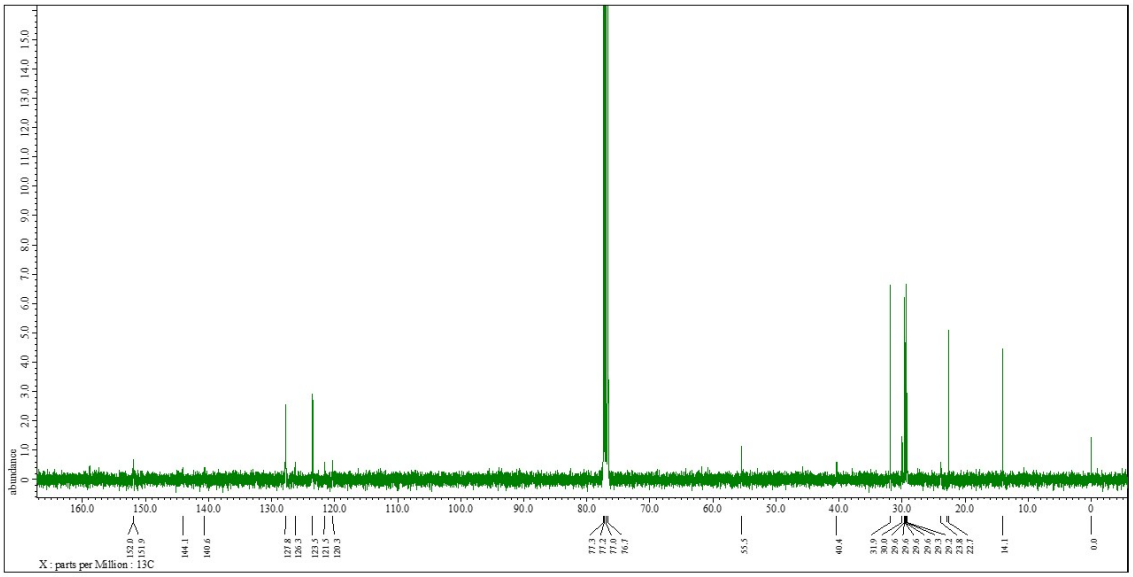

Chart S5. ^{13}C NMR spectrum of **N_fluo** in $CDCl_3$.

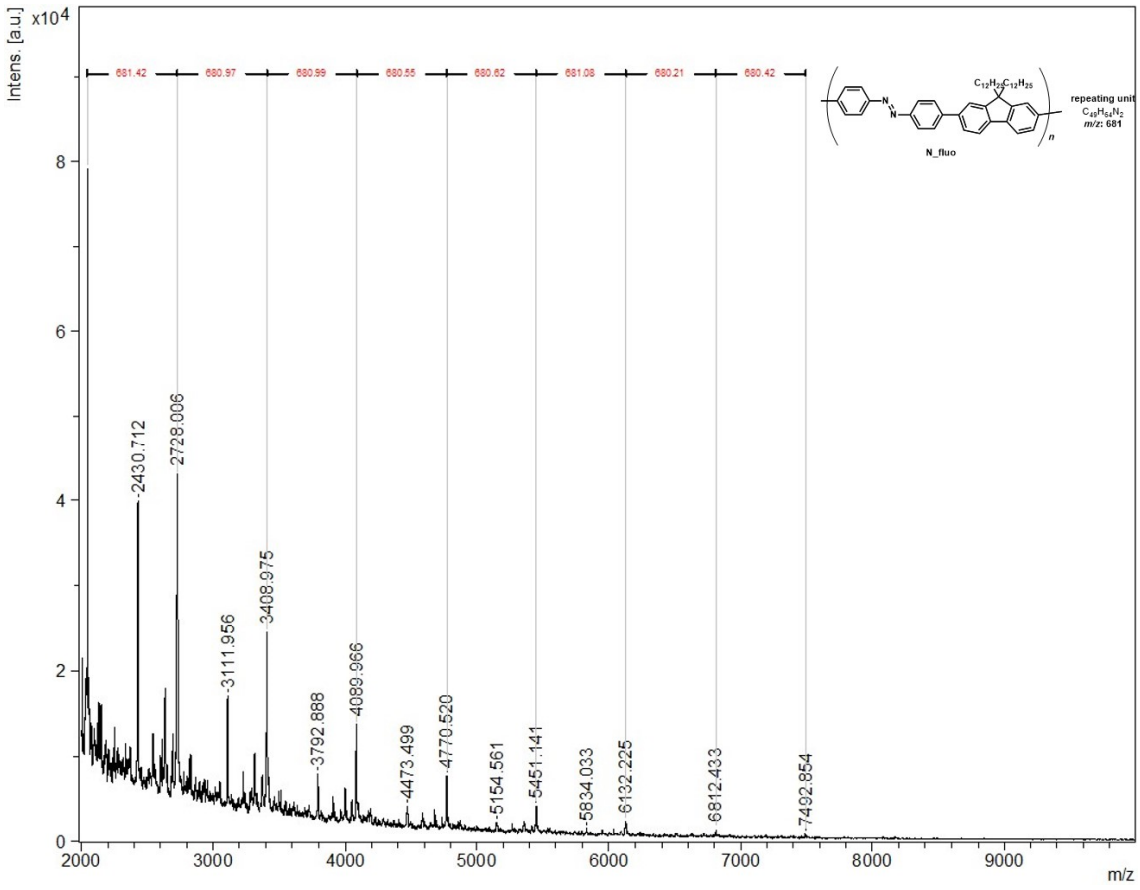

Chart S6. MALDI-TOFMS spectrum of **N_fluo** (matrix: DIT).

Synthesis of **C_bith**

A mixture of 4-bromo-*N*-[(4-bromophenyl)methylene]-benzenamine (**5**) (106 mg, 0.312 mmol), 5,5′-bis(trimethylstannyl)-3,3′-didodecyl-2,2′-bithiophene (**6**) (259 mg, 0.312 mmol), XPhos (8.9 mg, 0.018 mmol), $Pd_2(dba)_3$ (8.6 mg, 0.0094 mmol) was placed in a round-bottom flask equipped with a magnetic stirring bar. After degassing and filling N_2 three times, toluene (8.0 mL) was added to the mixture. The reaction was carried out at 80 °C for 48 h. atmosphere. After cooling to room temperature, the solution was purified by short column chromatography on SiO_2 and poured into a large amount of $CHCl_3$ to collect the polymer by filtration. The obtained polymer was redissolved in a small amount of $CHCl_3$, and then the product was reprecipitated from MeCN. The supernatant was removed with centrifugation (5000 rpm, 30 min) and following decantation. The precipitation was washed with MeCN and the supernatant was decanted off, repeatedly. The polymer was dried under vacuum to afford **C_bith** (204 mg, 96%) as a yellow film.

M_n = 13,000, M_w = 29,000, M_w/M_n = 2.2. ^{1}H NMR ($CDCl_3$, 400 MHz) δ 8.54 (s, 1H), 7.94 (d, J = 7.6 Hz, 2H), 7.75 (d, J = 8.0 Hz, 2H), 7.67 (d, J = 6.8 Hz, 2H), 7.38 (s, 1H), 7.28 (m, 3H), 2.61 (br, 6H), 1.65 (br, 4H), 1.25 (br, 32H), 0.88 (t, J = 7.2 Hz, 8H) ppm; ^{13}C NMR spectrum could not be obtained because the compound was decomposed during long term measurement.

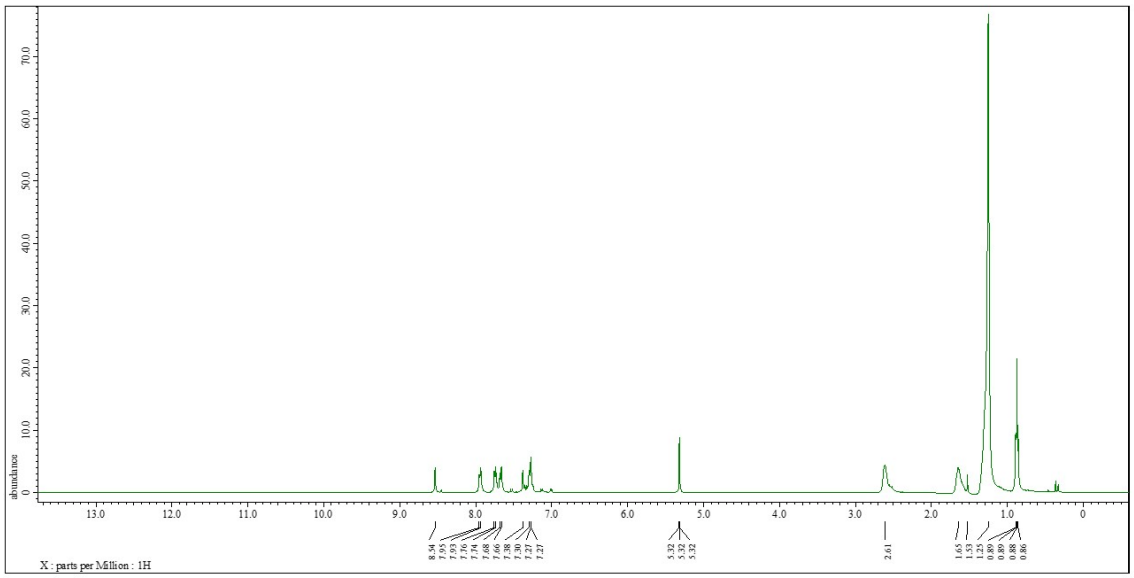

Chart S7. ^{1}H NMR spectrum of **C_bith** in CD_2Cl_2.

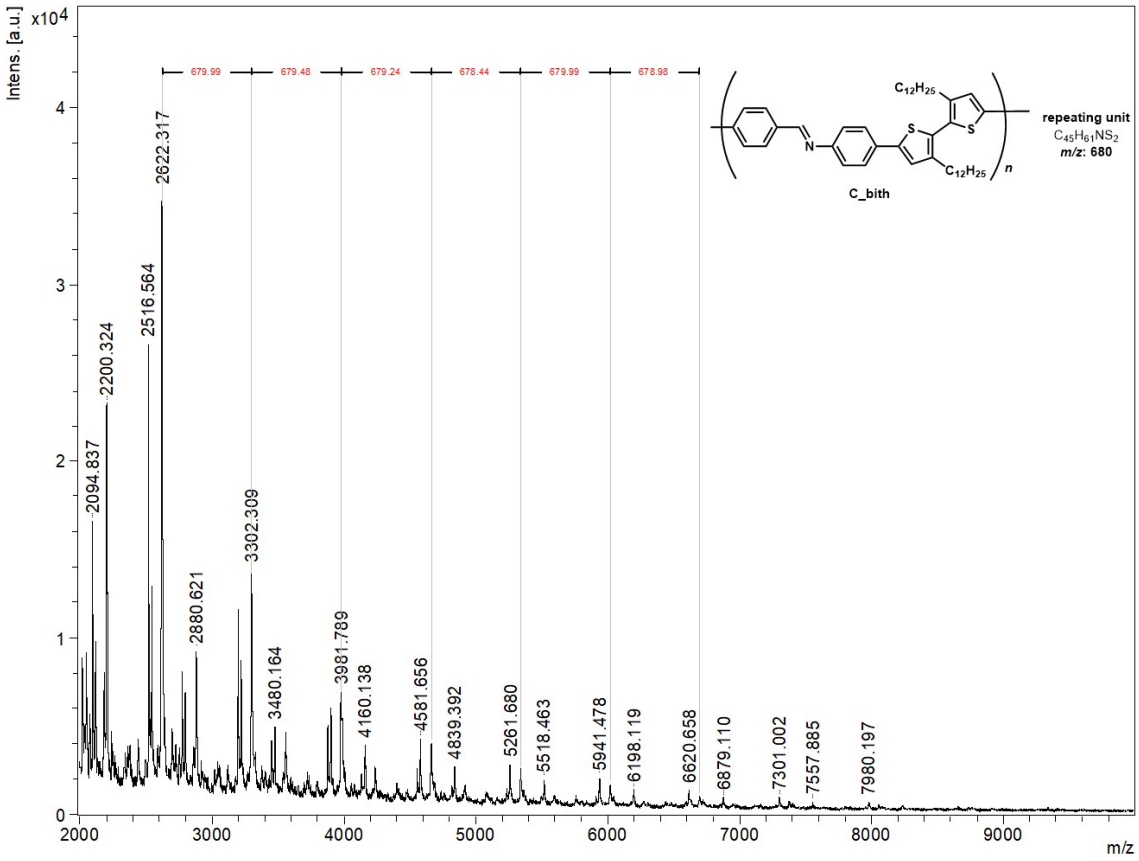

Chart S8. MALDI-TOFMS spectrum of **C_bith** (matrix: DCTB).

Cyclic voltammetry

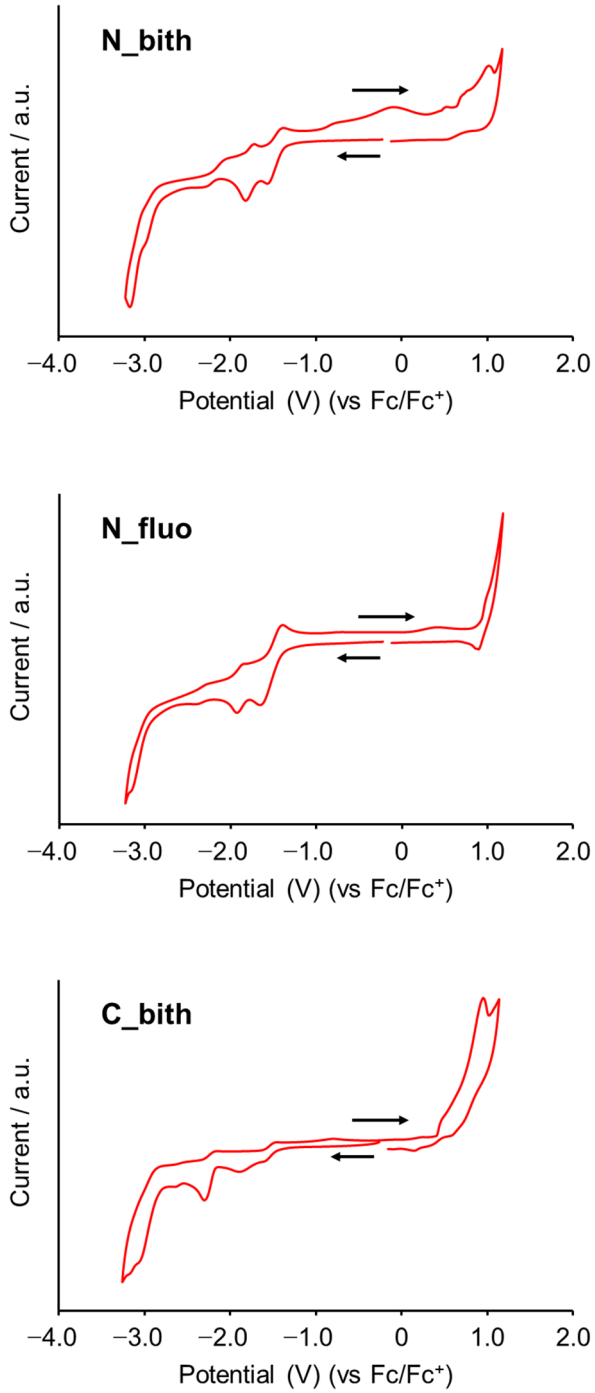

Chart S9. Cyclic voltammograms of **N_bith**, **N_fluo** and **C_bith** in THF (1.0×10^{-3} M per repeating unit) containing nBu$_4$NPF$_6$ (0.10 M) at room temperature with a scan rate of 0.1 V s^{-1}. The black arrows denote sweep directions (negative scan).

Results of GPC analysis

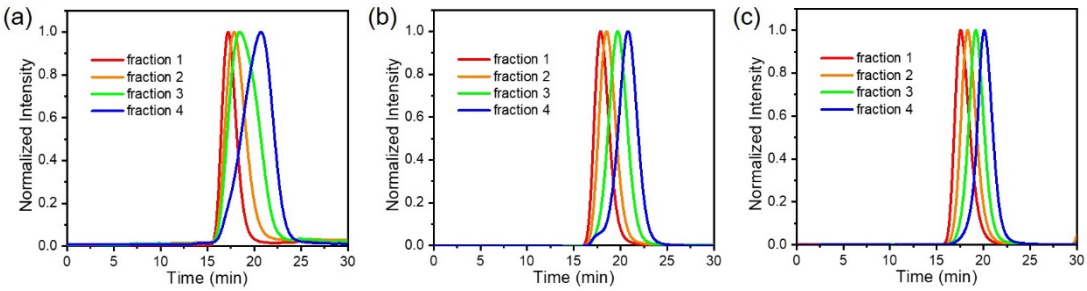

Figure S1. Normalized GPC chromatogram of (a) **N_bith**, (b) **N_fluo**, and (c) **C_bith** which were fractionated by preparative HPLC.

Table S1. The result of GPC analysis of fractionated **N_bith**

	M_n	M_w	PDI	n
fraction 1	63,000	110,000	1.7	92
fraction 2	34,000	63,000	1.9	50
fraction 3	19,000	41,000	2.2	28
fraction 4	9,000	20,000	2.2	13

Table S2. The result of GPC analysis of fractionated **N_fluo**

	M_n	M_w	PDI	n
fraction 1	36,000	55,000	1.5	53
fraction 2	24,000	36,000	1.5	36
fraction 3	13,000	19,000	1.4	19
fraction 4	7,100	12,000	1.7	10

Table S3. The result of GPC analysis of fractionated **C_bith**

	M_n	M_w	PDI	n
fraction 1	42,000	69,000	1.7	62
fraction 2	27,000	40,000	1.5	39
fraction 3	17,000	24,000	1.4	24
fraction 4	11,000	14,000	1.3	16

Solvent effect of polymers

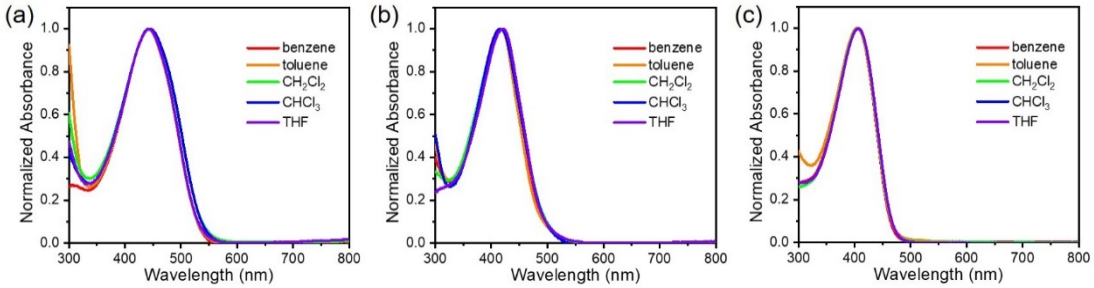

Figure S2. UV–vis absorption spectra of (a) **N_bith**, (b) **N_fluo**, and (c) **C_bith** in mixed solvents of $CHCl_3$/each solvent (1/99, v/v) (1.0×10^{-5} M per repeating units of the polymers).

Results of TGA

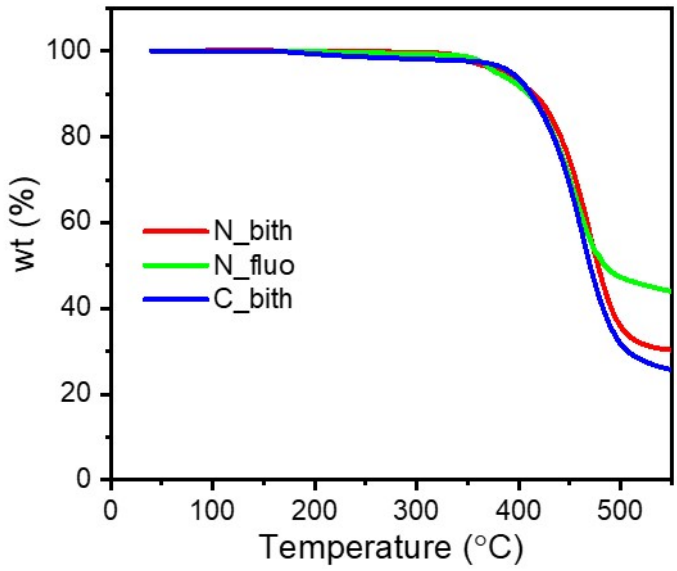

Figure S3. TGA curves of **N_bith**, **N_fluo**, and **C_bith**.

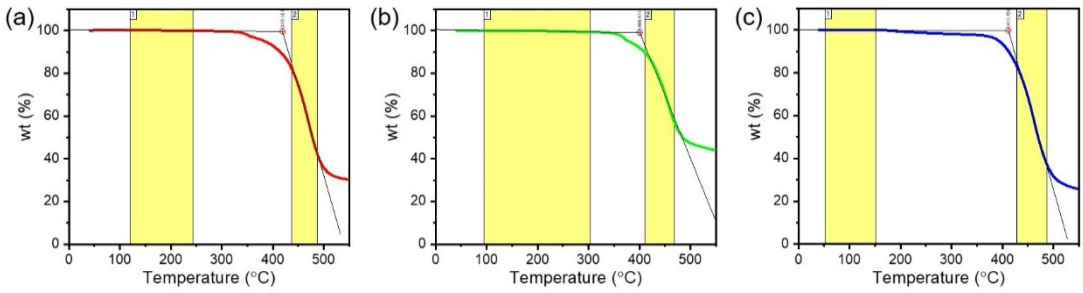

Figure S4. Analyzed TGA curves of (a) **N_bith**, (b) **N_fluo**, and (c) **C_bith**.

Table S4. The result of TGA of three polymers.

sample	T_d[a] /°C	T_{d5}[b] /°C	T_{d50}[c] /°C
N_bith	419	385	478
N_fluo	400	378	485
C_bith	412	393	470

[a] Determined from tangents intersection of TGA curve shown in Figure S4.

[b] Determined at 5 wt% weight losses in the TGA curve.

[c] Determined at 50 wt% weight losses in the TGA curve.

UV–vis absorption spectra in $CHCl_3$ and film state with TFA

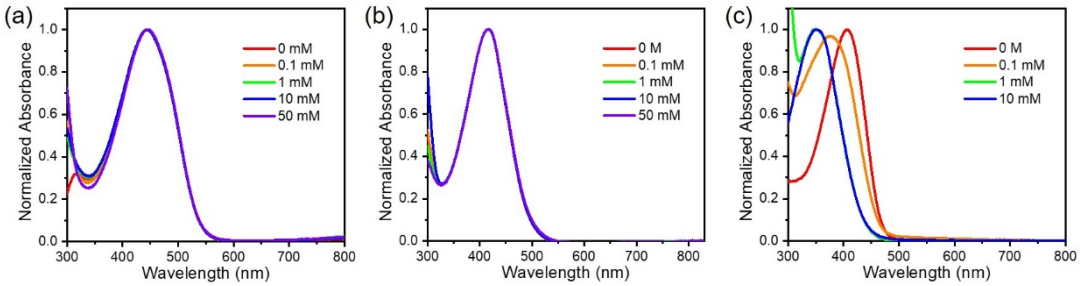

Figure S5. UV–vis absorption spectra of (a) **N_bith**, (b) **N_fluo**, and (c) **C_bith** in $CHCl_3$ (1.0×10^{-5} M per repeating units of the polymers) with each concentration of TFA.

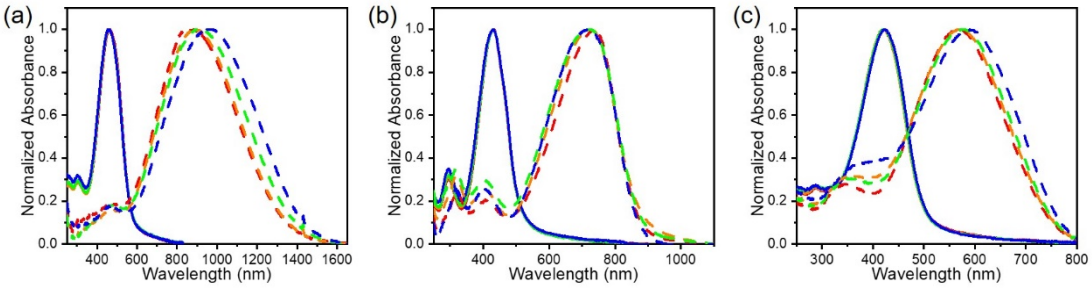

Figure S6. UV–vis absorption spectra in film state of (a) **N_bith** (solid line: pristine film, dashed line: exposing TFA vapor), (b) **N_fluo** (solid line: pristine film, dashed line: exposing TFA vapor), and (c) **C_bith** (solid line: pristine film, dashed line: after exposed TFA vapor). These film samples were prepared via the spin-coating (1000 rpm, 30 seconds) on the quartz substrate with $CHCl_3$ (1 mg/300 μL). Red lines show fraction 1, orange lines show fraction 2, green lines show fraction 3, and blue lines show fraction 4. The molecular weights are listed in Tables S1–S3.

Photographic images of the polymer films

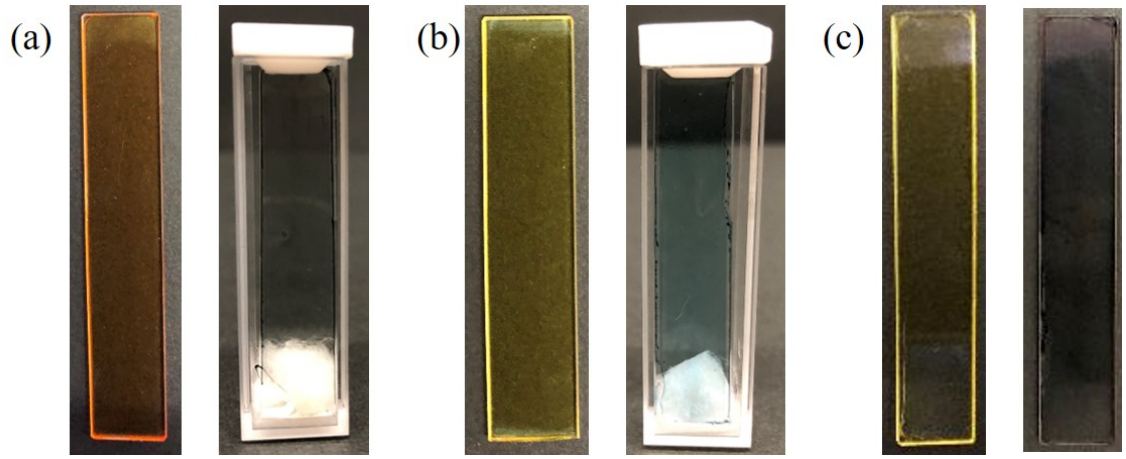

Figure S7. Photographic image of the pristine film (left) and TFA vapor exposing or exposed film (right) of (a) **N_bith**, (b) **N_fluo**, and (c) **C_bith**.

Results of ^{1}H NMR spectra and GPC chromatograms after exposure to TFA vapor in film state

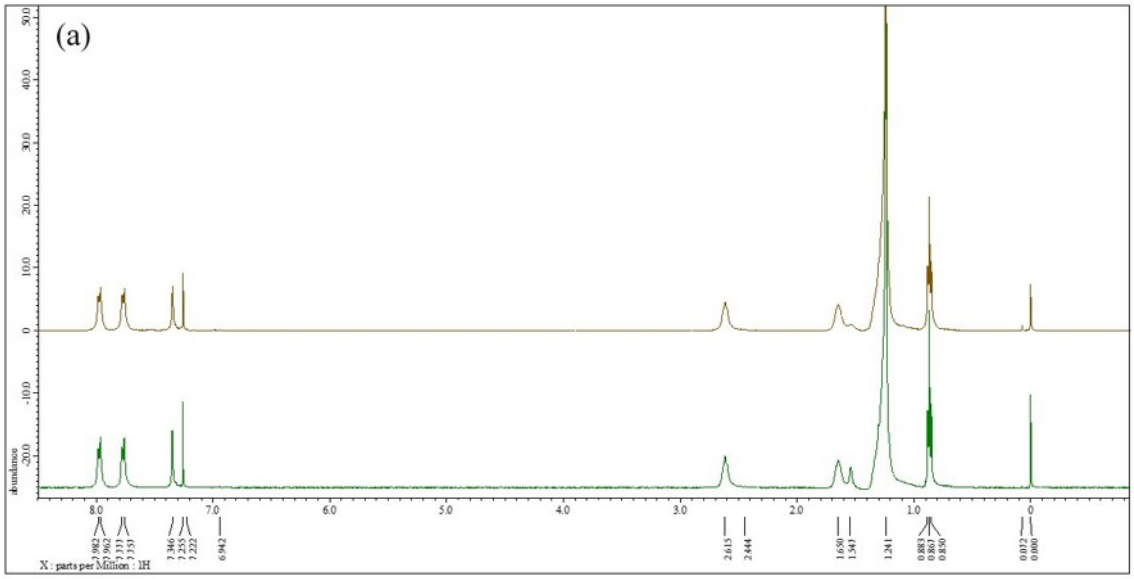

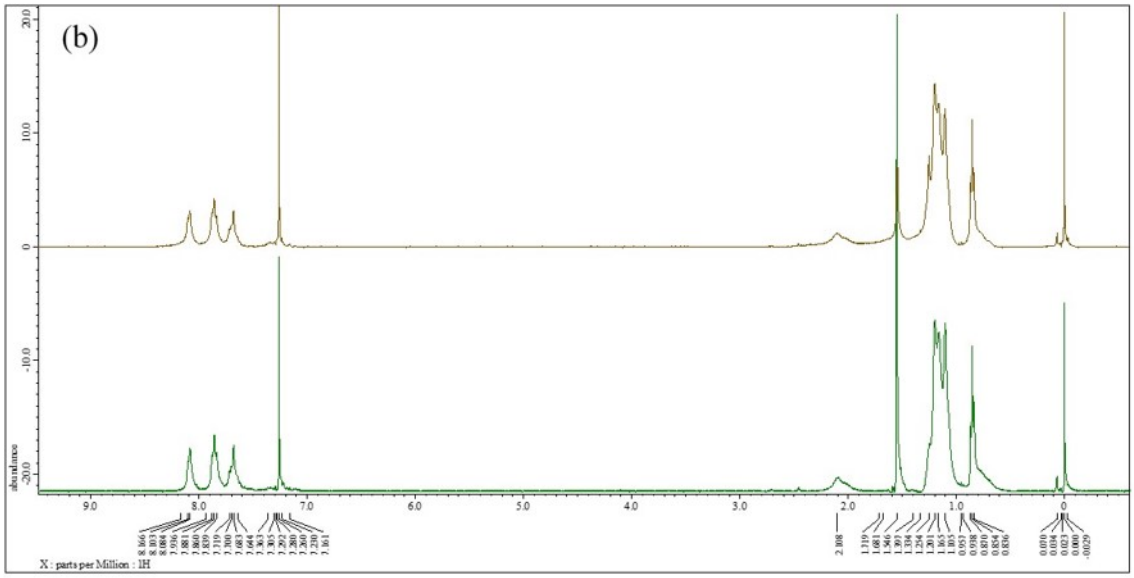

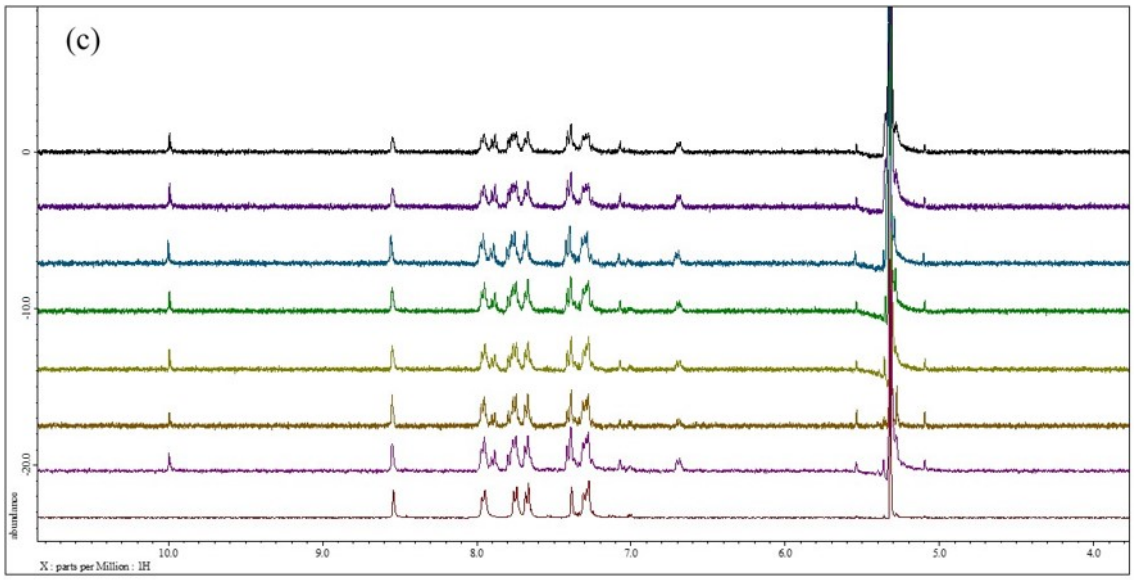

Figure S8. ^{1}H NMR spectra of (a) **N_bith**, (b) **N_fluo** in $CDCl_3$ (green : purified sample, red : exposure to TFA vapor in film state, and then redissolved in CD_2Cl_2), and (c) **C_bith** in CD_2Cl_2 (red solid line: sample that was not exposed TFA vapor, pink to black solid line: sample that was exposed TFA vapor for 3 seconds, liberated to the atmosphere[a] for 0 min, 1 min, 5min, 10 min, 30 min, 60 min, and 180 min and then redissolved in CD_2Cl_2).

[a] temperature : at 19.4 °C, humidity : 28.1%).

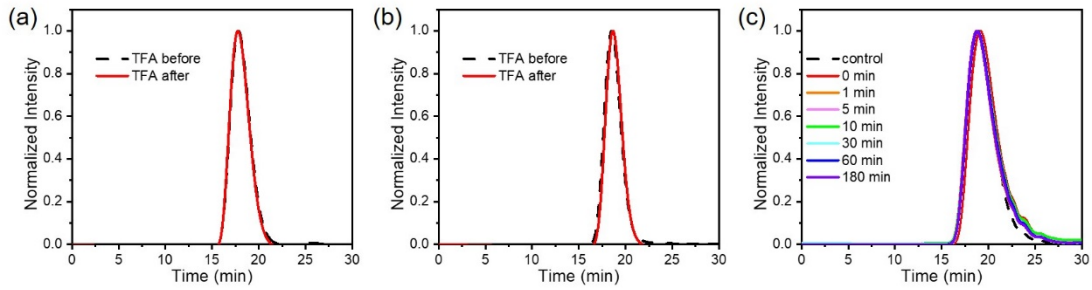

Figure S9. GPC chromatograms in $CHCl_3$ of (a) **N_bith**, (b) **N_fluo** (black dashed line: sample that was not exposed TFA vapor, red solid line: sample that was exposed TFA vapor for 3 seconds and redissolved in $CHCl_3$), and (c) **C_bith** (black dashed line: sample that was not exposed TFA vapor, red to purple solid line: sample that was exposed TFA vapor for 3 seconds, liberated to the atmosphere[a] for each time, and then redissolved in $CHCl_3$).

[a] temperature : at 19.4 °C, humidity : 28.1%

Table S5. The results of GPC chromatograms of **N_bith** before and after exposure to TFA vapor

	M_n	M_w	PDI	n
TFA before	34,000	63,000	1.9	50
TFA after	35,000	68,000	2.0	51

Table S6. The results of GPC chromatograms of **N_fluo** before and after exposure to TFA vapor

	M_n	M_w	PDI	n
TFA before	24,000	36,000	1.5	36
TFA after	24,000	35,000	1.4	35

Table S7. The results of GPC chromatograms of **C_bith** before exposure to TFA vapor and after exposure to TFA vapor and liberated to the atmosphere for each time

	M_n	M_w	PDI	n
TFA before	13,000	29,000	2.2	19
0 min	11,000	26,000	2.4	16
1 min	11,000	34,000	3.0	16
5 min	12,000	32,000	2.7	17
10 min	12,000	32,000	2.8	17
30 min	11,000	31,000	2.7	17
60 min	11,000	31,000	2.9	16
180 min	11,000	32,000	2.9	17

Table S8. The ratio of remaining portion of imine structure after exposure to TFA vapor for 3 seconds and liberated to the atmosphere for each time obtained from NMR spectra[a]

	0 min	1 min	5 min	10 min	30 min	60 min	180 min
ratio (%)	75	68	66	64	66	57	57

[a] Obtained by dividing the integral value of the peak of imine (at 8.55 ppm) by the sum of the integral values of the peaks of aldehyde (at 10.00 ppm) and imine.

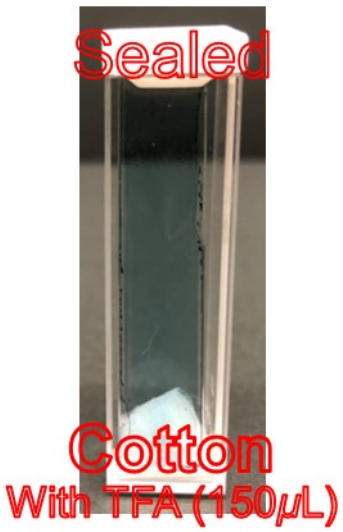

Figure S10. Photographic image of measurement method of **N_bith** and **N_fluo** film exposing TFA vapor. The illustrated film is **N_fluo**.

Computational details for theoretical calculation

The Gaussian 16 program package[6] was used for computation. We optimized the structures of the structures of neutral state (**N_bith'**, **N_fluo'** and **C_bith'**) and protonated state (**N_bith+'**, **N_fluo+'** and **C_bith+'**) which are model compounds of three polymers in the ground S_0 states and calculated their molecular orbitals. The density functional theory (DFT) was applied for the optimization of the structures in the S_0 states at B3LYP/6-31+G(d,p) and CAM-B3LYP/6-31+G(d,p) levels. We calculated the energy of the transitions with optimized geometries in the S_0 states by time-dependent (TD) DFT at B3LYP/6-31+G(d,p) and CAM-B3LYP/6-31+G(d,p) levels, respectively. The CAM (Coulomb-attenuating method)-B3LYP is a functional combines the hybrid features of B3LYP and the long-range correction. The functional was designed to get over the difficulties including: (i) the polarizability of long chains, (ii) excitations for Rydberg states, (iii) charge transfer excitations.[7] Therefore, we performed DFT calculation using these two functions.

In Table S9 and S10, positive and negative CIS coefficients represent excitation and de-excitation, respectively.[8],[9]

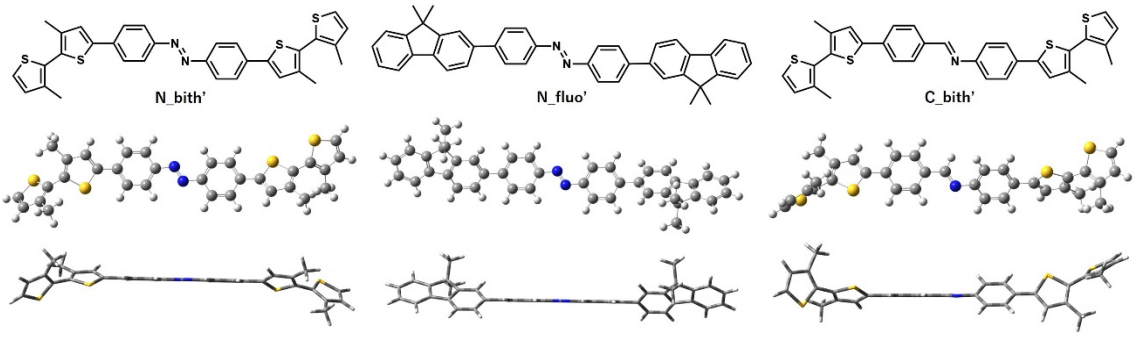

Figure S11. Optimized structures of **N_bith'**, **N_fluo'** and **C_bith'** at B3LYP/6-31+G(d,p).

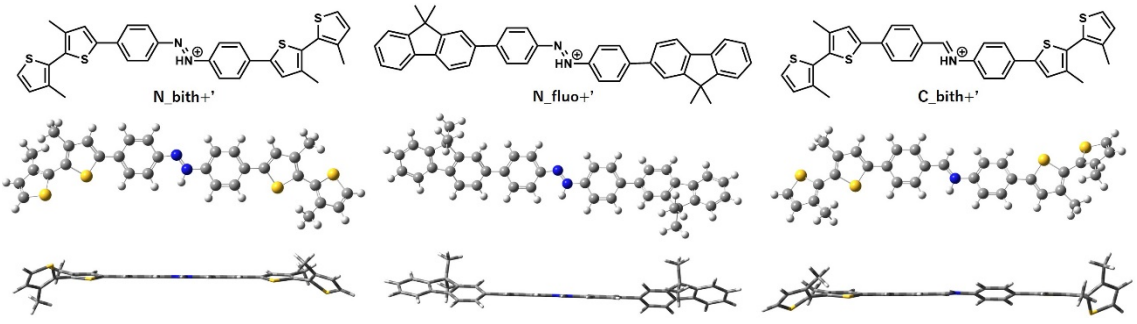

Figure S12. Optimized structures of **N_bith+'**, **N_fluo+'** and **C_bith+'** at B3LYP/6-31+G(d,p).

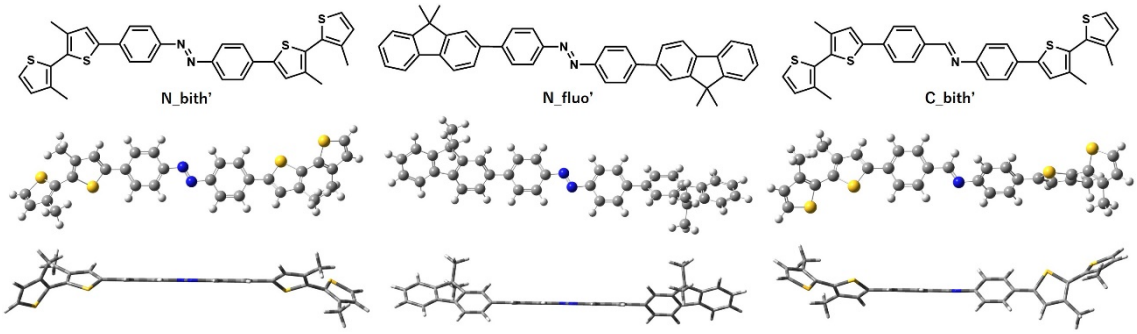

Figure S13. Optimized structures of **N_bith'**, **N_fluo'** and **C_bith'** at CAM-B3LYP/6-31+G(d,p).

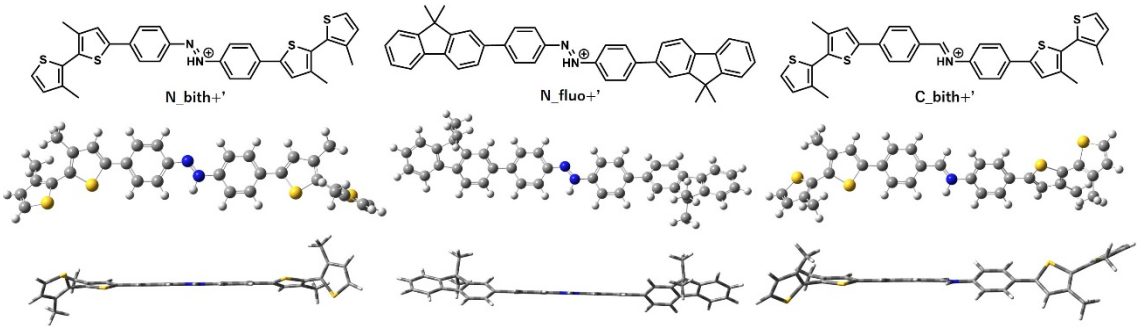

Figure S14. Optimized structures of **N_bith+'**, **N_fluo+'** and **C_bith+'** at CAM-B3LYP/6-31+G(d,p).

Table S9. The results of TD-DFT calculations at B3LYP/6-31+G(d,p) for **N_bith'** and **N_bith+'** (*f*: oscillator strength)

excited state	**N_bith'**	**N_bith+'**
S_1	498.24 nm, f = 0.0125 HOMO−2→LUMO (n→π*) (95%) HOMO−2→LUMO+2 (2.2%)	902.17 nm, f = 1.7196 HOMO→LUMO (103%)[a] HOMO←LUMO (4.6%)[b]
S_2	481.68 nm, f = 1.8468 HOMO→LUMO (π→π*) (98%)	681.58 nm, f = 0.2553 HOMO−1→LUMO (96%)

[a] excitation

[b] de-excitation

Table S10. The results of TD-DFT calculations at B3LYP/6-31+G(d,p) for **N_fluo'** and **N_fluo+'** (*f*: oscillator strength)

excited state	**N_fluo'**	**N_fluo+'**

S_1	490.54 nm, f = 0.0000 HOMO−2→LUMO (n→π*) (97%) HOMO−2→LUMO+2 (2.3%)	931.88 nm, f = 1.4150 HOMO→LUMO (102%)[a] HOMO←LUMO (2.4%)[b]
S_2	448.04 nm, f = 1.8606 HOMO→LUMO (π→π*) (99%)	694.82 nm, f = 0.4007 HOMO−1→LUMO (98%)

[a] excitation

[b] de-excitation

Table S11. The results of TD-DFT calculations at B3LYP/6-31+G(d,p) for **C_bith'** and **C_bith+'** (*f*: oscillator strength)

excited state	**C_bith'**	**C_bith+'**
S_1	436.66 nm, f = 1.3407 HOMO→LUMO (97%)	833.80 nm, f = 1.0300 HOMO→LUMO (100%)
S_2	368.37 nm, f = 0.4683 HOMO−1→LUMO (93%) HOMO→LUMO+1 (3.8%)	619.85 nm, f = 0.8154 HOMO−1→LUMO (96%)

Table S12. The results of TD-DFT calculations at CAM-B3LYP/6-31+G(d,p) for **N_bith'** and **N_bith+'** (*f*: oscillator strength)

excited state	**N_bith'**	**N_bith+'**
S_1	450.24 nm, f = 0.0001 HOMO−6→LUMO (4.3%) HOMO−5→LUMO (9.3%) HOMO−4→LUMO (n→π*) (70%) HOMO−4→ LUMO+2 (4.9%)	642.71 nm, f = 2.1197 HOMO−1→LUMO (11%) HOMO→LUMO (82%)
S_2	372.81 nm, f = 2.1200 HOMO−2→LUMO (2.8%) HOMO−1→LUMO+1 (4.9%) HOMO→LUMO (π→π*) (85%)	490.86 nm, f = 0.0669 HOMO−3→LUMO (6.1%) HOMO−1→LUMO (80%) HOMO→LUMO (9.3%)

Table S13. The results of TD-DFT calculations at CAM-B3LYP/6-31+G(d,p) for **N_fluo'** and **N_fluo+'** (*f*: oscillator strength)

excited state	**N_fluo'**	**N_fluo+'**
S_1	447.56 nm, f = 0.0000 HOMO−3→LUMO (n→π*) (87%) HOMO−3→LUMO+2 (6.4%)	639.12 nm, f = 1.8868 HOMO−5→LUMO (5.4%) HOMO−1→LUMO (11%) HOMO→LUMO (81%)
S_2	354.66 nm, f = 2.3740 HOMO−2→LUMO (12%) HOMO−1→LUMO+1 (4.7%) HOMO→LUMO (π→π*) (79%)	511.60 nm, f = 0.1577 HOMO−1→LUMO (84%) HOMO→LUMO (13%)

Table S14. The results of TD-DFT calculations at CAM-B3LYP/6-31+G(d,p) for **C_bith'** and **C_bith+'** (*f*: oscillator strength)

excited state	**C_bith'**	**C_bith+'**
S_1	344.58 nm, f = 1.9293 HOMO−2→LUMO (4.9%) HOMO−1→LUMO (5.5%) HOMO−1→LUMO+1 (5.5%) HOMO→LUMO (71%) HOMO→LUMO+1 (3.5%)	519.41 nm, f = 1.8042 HOMO–3→LUMO (3.3%) HOMO–1→LUMO (25%) HOMO→LUMO (63%)
S_2	300.32 nm, f = 0.1482 HOMO−11→LUMO (3.0%) HOMO−9→LUMO (2.4%) HOMO−4→LUMO (2.9%) HOMO−2→LUMO (3.3%) HOMO−1→LUMO (60%) HOMO→LUMO+1 (11%)	437.70 nm, f = 0.1035 HOMO−1→LUMO (66%) HOMO→LUMO (25%)

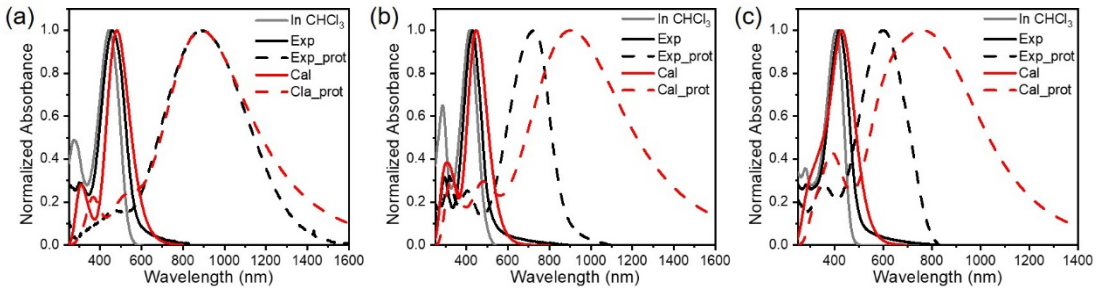

Figure S15. Experimental UV–vis absorption spectra (solid line) and calculated TD-DFT absorption spectra (dashed line) of (a) **N_bith** (b) **N_fluo**, and (c) **C_bith**. (black: pristine film, red: exposing TFA vapor, and gray solid line: in $CHCl_3$ (1.0×10^{-5})). TD-DFT was performed using Gaussian16A.03 package at (TD-)B3LYP/6-31+G(d,p).

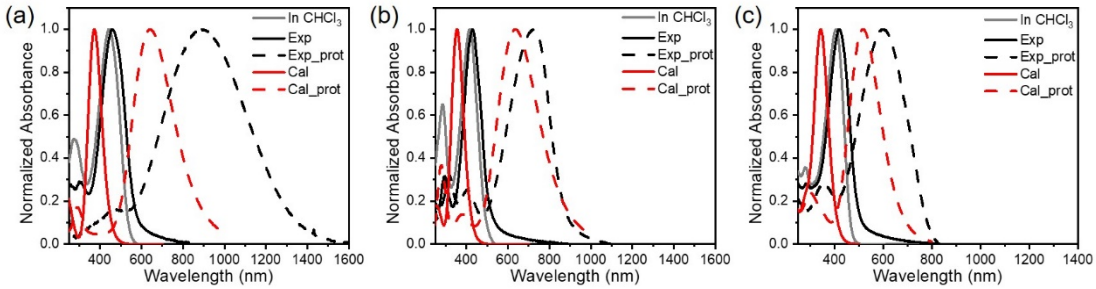

Figure S16. Experimental UV–vis absorption spectra (solid line) and calculated TD-DFT absorption spectra (dashed line) of (a) **N_bith** (b) **N_fluo**, and (c) **C_bith**. (black : pristine film, red : exposing TFA vapor, and gray solid line: in $CHCl_3$ (1.0×10^{-5})). TD-DFT was performed using Gaussian16A.03 package at (TD-)CAM-B3LYP/6-31+G(d,p).

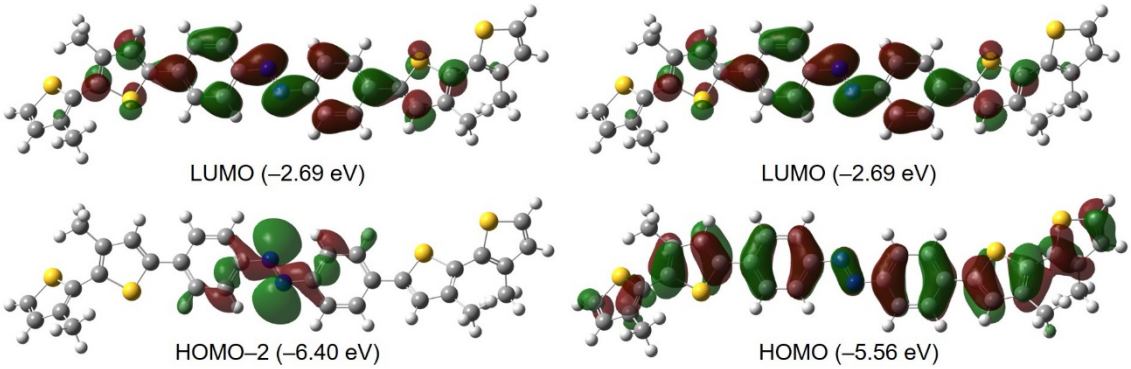

Figure S17. Selected FMOs of **N_bith'** that have main contribution in the S_0–S_1 (left) and S_0–S_2 (right) transition obtained by B3LYP/6-31+G(d,p) level (isovalue = 0.02).

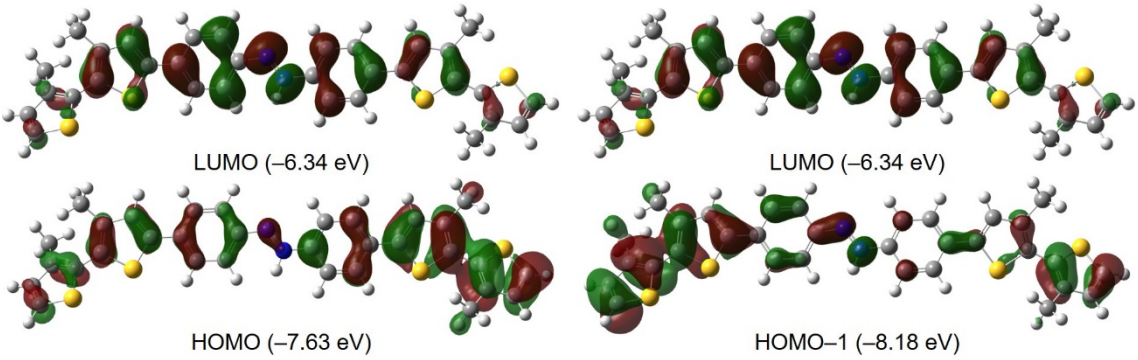

Figure S18. Selected FMOs of **N_bith+'** that have main contribution in the S_0–S_1 (left) and S_0–S_2 (right) transition obtained by B3LYP/6-31+G(d,p) level (isovalue = 0.02).

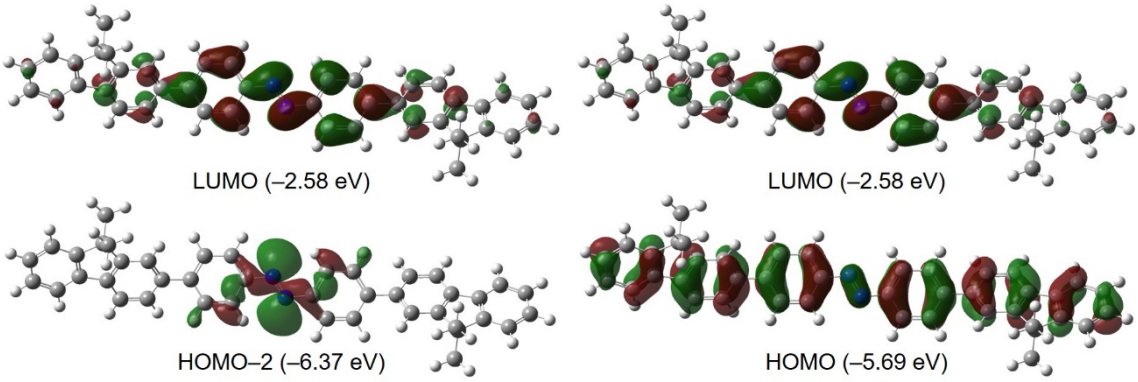

Figure S19. Selected FMOs of **N_fluo'** that have main contribution in the S_0–S_1 (left) and S_0–S_2 (right) transition obtained by B3LYP/6-31+G(d,p) level (isovalue = 0.02).

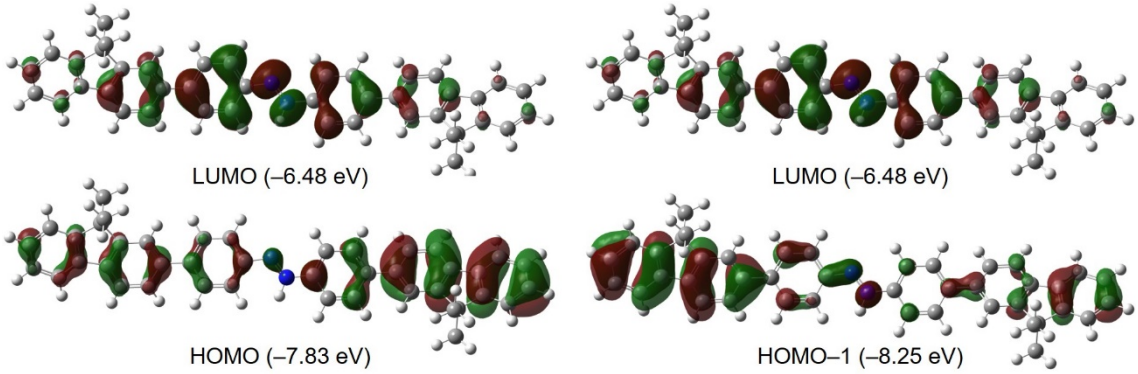

Figure S20. Selected FMOs of **N_fluo+'** that have main contribution in the S_0–S_1 (left) and S_0–S_2 (right) transition obtained by B3LYP/6-31+G(d,p) level (isovalue = 0.02).

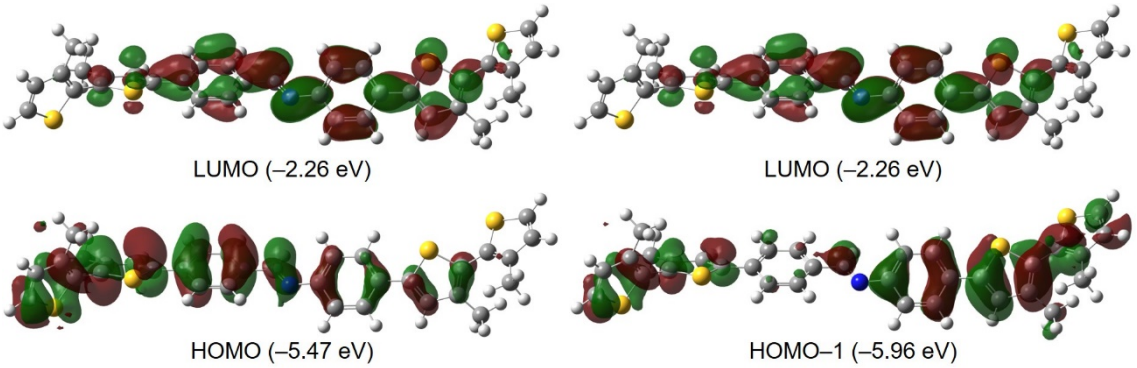

Figure S21. Selected FMOs of **C_bith'** that have main contribution in the S_0–S_1 (left) and S_0–S_2 (right) transition obtained by B3LYP/6-31+G(d,p) level (isovalue = 0.02).

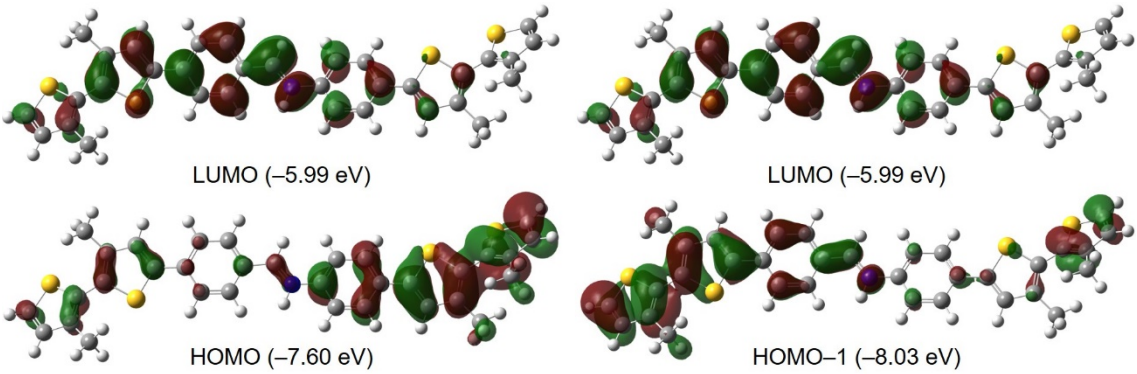

Figure S22. Selected FMOs of **C_bith+'** that have main contribution in the S_0–S_1 (left) and S_0–S_2 (right) transition obtained by B3LYP/6-31+G(d,p) level (isovalue = 0.02).

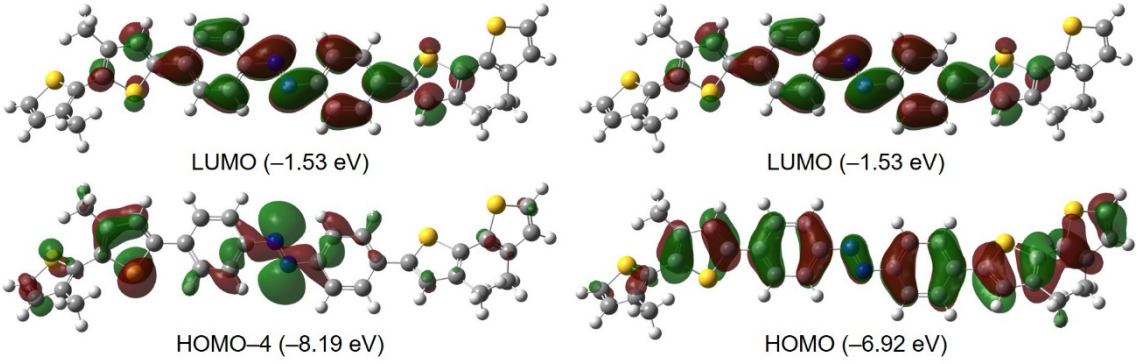

Figure S23. Selected FMOs of **N_bith'** that have main contribution in the S_0–S_1 (left) and S_0–S_2 (right) transition obtained by CAM-B3LYP/6-31+G(d,p) level (isovalue = 0.02).

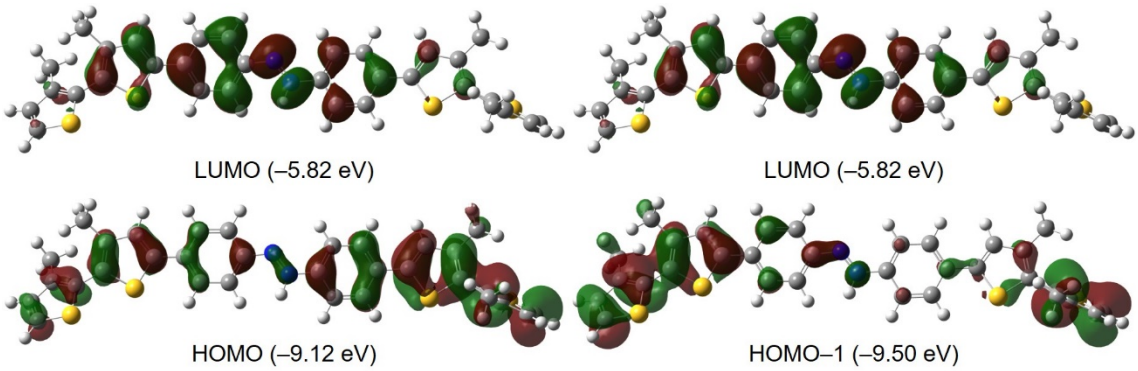

Figure S24. Selected FMOs of **N_bith+'** that have main contribution in the S_0–S_1 (left) and S_0–S_2 (right) transition obtained by CAM-B3LYP/6-31+G(d,p) level (isovalue = 0.02).

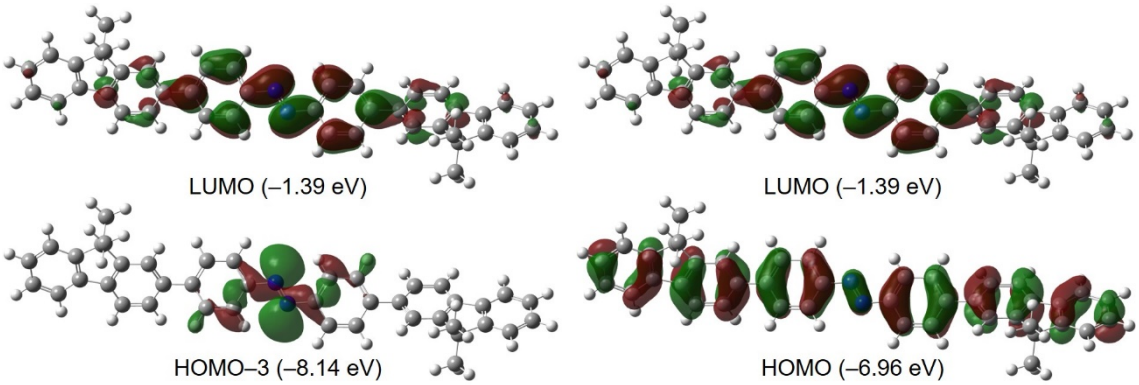

Figure S25. Selected FMOs of **N_fluo'** that have main contribution in the S_0–S_1 (left) and S_0–S_2 (right) transition obtained by CAM-B3LYP/6-31+G(d,p) level (isovalue = 0.02).

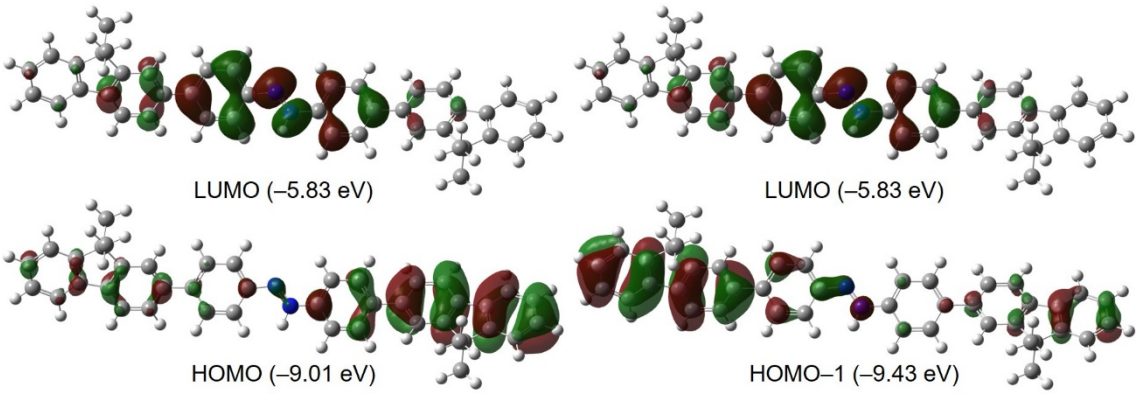

Figure S26. Selected FMOs of **N_fluo+'** that have main contribution in the S_0–S_1 (left) and S_0–S_2 (right) transition obtained by CAM-B3LYP/6-31+G(d,p) level (isovalue = 0.02).

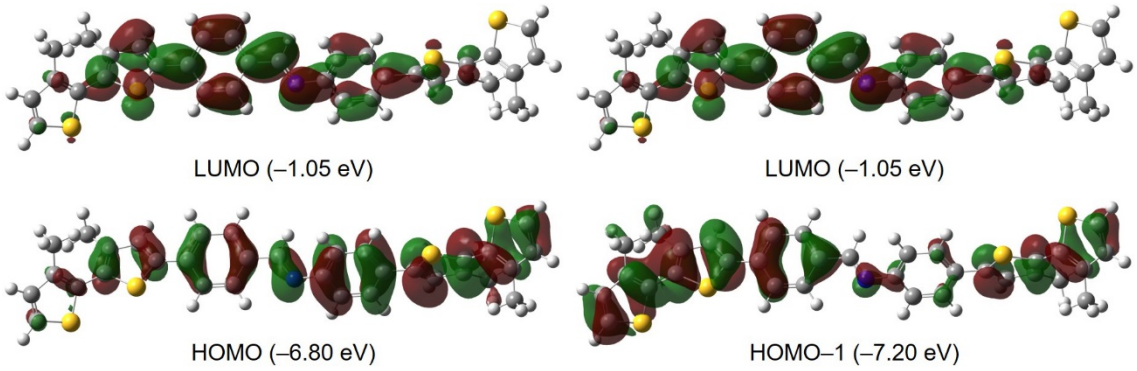

Figure S27. Selected FMOs of **C_bith'** that have main contribution in the S_0–S_1 (left) and S_0–S_2 (right) transition obtained by CAM-B3LYP/6-31+G(d,p) level (isovalue = 0.02).

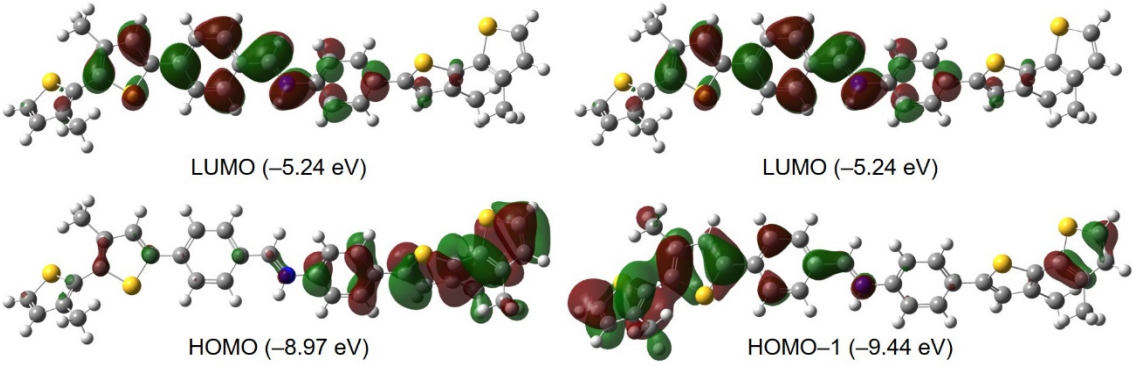

Figure S28. Selected FMOs of **C_bith+'** that have main contribution in the S_0–S_1 (left) and S_0–S_2 (right) transition obtained by CAM-B3LYP/6-31+G(d,p) level (isovalue = 0.02).

Detection of various acids

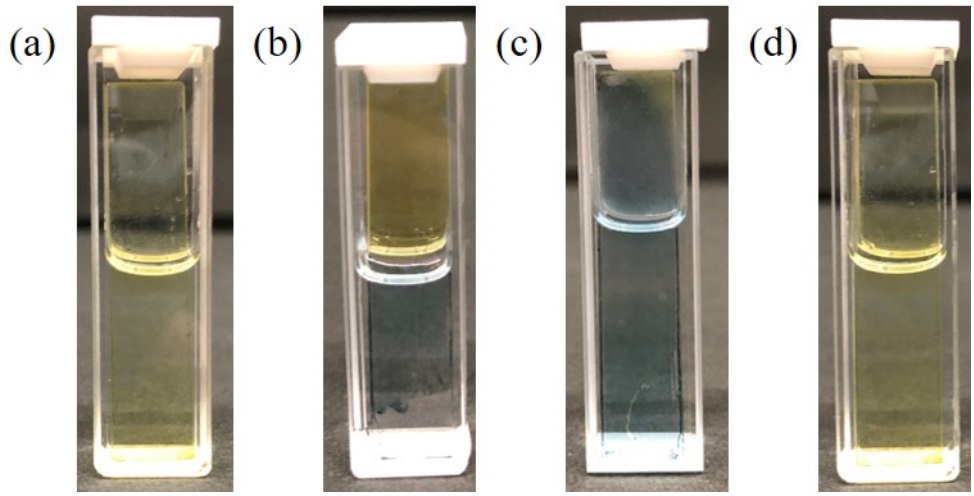

Figure S29. Photographic image of **N_fluo** film dipped into (a) HCl, (b) H_2SO_4 (c) HNO_3, and (d) CH_3COOH.

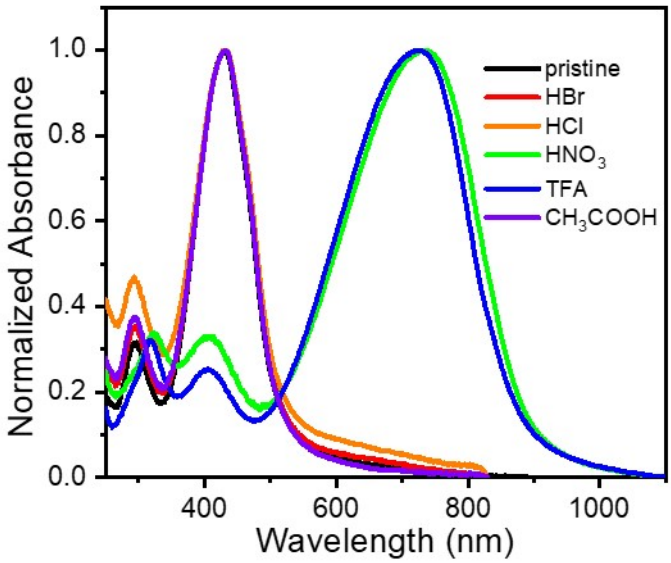

Figure S30. UV–vis absorption spectra in film state of **N_fluo** exposing acid vapors (black: pristine film, red: HBr vapor, orange: HCl vapor, green : HNO_3 vapor, blue: TFA vapor, and purple: CH_3COOH vapor. We could not measure H_2SO_4 vapor because it melted the cotton and emitted toxic smoke.)

References

[1] W. Zhang, K. Yoshida, M. Fujiki, X. Zhu, *Macromolecules* **2011**, *44*, 5105.

[2] Q. Liu, G. Li, Z. Tang, L. Chen, B. Liao, B. Ou, Z. Zhou, H. Zhou, *Mater. Chem. Phys.* **2017**, *186*, 11.

[3] X. Guo, Q. Liao, E. F. Manley, Z. Wu, Y. Wang, W. Wang, T. Yang, Y.-E. Shin, X. Cheng, Y. Liang, L. X. Chen, K.-J. Baeg, T. J. Marks, X. Guo, *Chem. Mater.* **2016**, *28*, 2449.

[4] R. Yoshii, K. Tanaka, Y. Chujo, *Macromolecules* **2014**, *47*, 2268.

[5] Gon, M.; Tanaka, K.; Chujo, Y. *Angew. Chem. Int. Ed.* **2018**, *57*, 6546–6551.

[6] Gaussian 16, Revision C.01, M. J. Frisch, G. W. Trucks, H. B. Schlegel, G. E. Scuseria, M. A. Robb, J. R. Cheeseman, G. Scalmani, V. Barone, G. A. Petersson, H. Nakatsuji, X. Li, M. Caricato, A. V. Marenich, J. Bloino, B. G. Janesko, R. Gomperts, B. Mennucci, H. P. Hratchian, J. V. Ortiz, A. F. Izmaylov, J. L. Sonnenberg, D. Williams-Young, F. Ding, F. Lipparini, F. Egidi, J. Goings, B. Peng, A. Petrone, T. Henderson, D. Ranasinghe, V. G. Zakrzewski, J. Gao, N. Rega, G. Zheng, W. Liang, M. Hada, M. Ehara, K. Toyota, R. Fukuda, J. Hasegawa, M. Ishida, T. Nakajima, Y. Honda, O. Kitao, H. Nakai, T. Vreven, K. Throssell, J. A. Montgomery, Jr., J. E. Peralta, F. Ogliaro, M. J. Bearpark, J. J. Heyd, E. N. Brothers, K. N. Kudin, V. N. Staroverov, T. A. Keith, R. Kobayashi, J. Normand, K. Raghavachari, A. P. Rendell, J. C. Burant, S. S. Iyengar, J. Tomasi, M. Cossi, J. M. Millam, M. Klene, C. Adamo, R. Cammi, J. W. Ochterski, R. L. Martin, K. Morokuma, O. Farkas, J. B. Foresman, D. J. Fox, Gaussian, Inc., Wallingford CT, 2016.

[7] S. Temel, C. Alasalvar, H. Eserci, E. Agar, *J. Mol. Struct.* **2017**, *1128*, 5.

[8] F. Cordova, L. J. Doriol, A. Ipatov, M. E. Casida, *J. Chem. Phys.* **2007**, *127*, 164111.

[9] M. E. Casida, M. Huix-Rotllant, *Annu. Rev. Phys. Chem.* **2012**, *63*, 287.